Live-imaging *twin1* and M0171>*bdl* phenotypes in *in-vitro* cultured *Arabidopsis thaliana* ovules with fluorescent markers

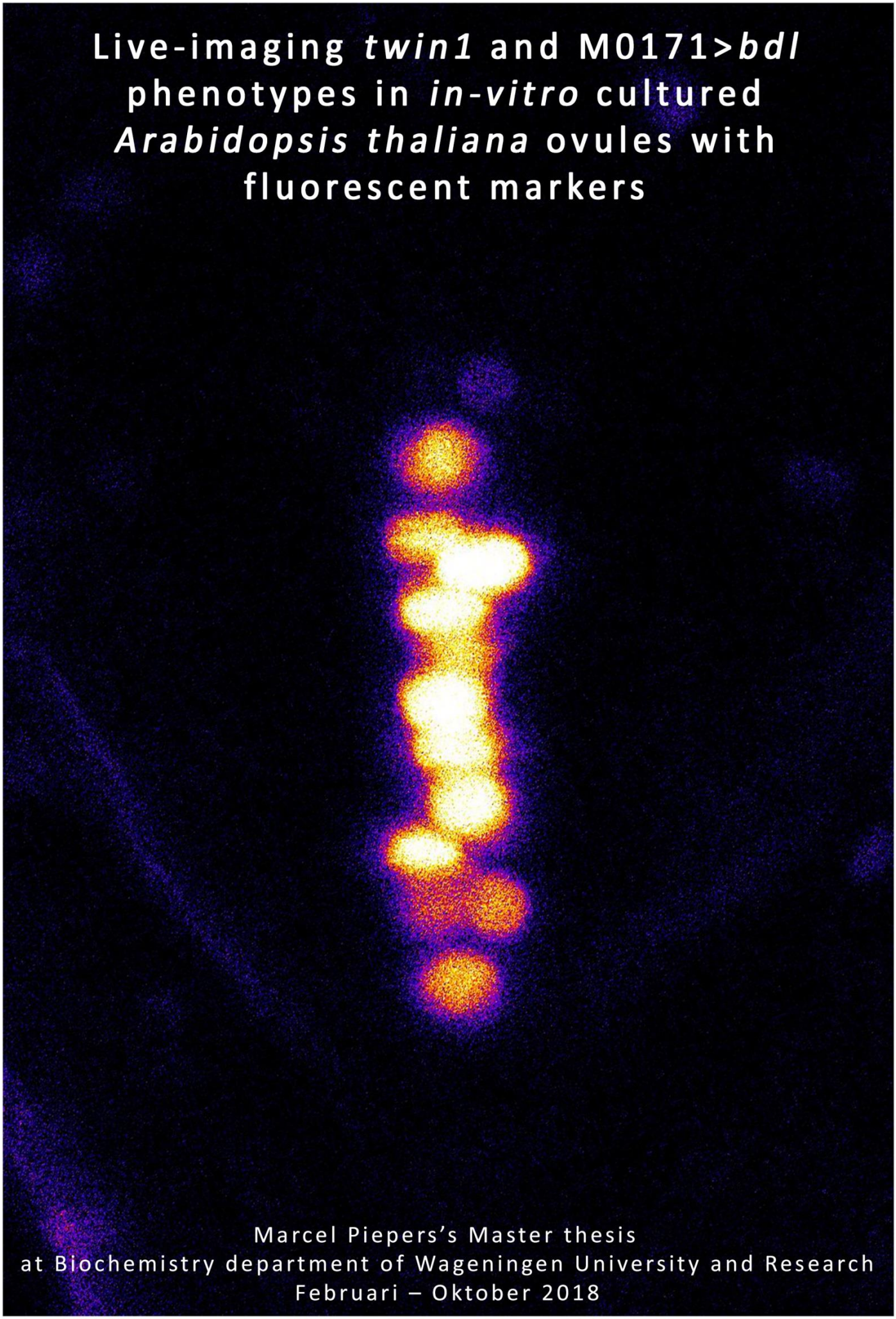

Marcel Piepers's Master thesis
at Biochemistry department of Wageningen University and Research
Februari – Oktober 2018

Abstract

Next to zygotic embryogenesis, plants possess the capability to derive embryos from somatic cells. Suspensor cells, which are located below the zygote-derived embryo are somatic cells capable of undergoing such transformation. During the onset of suspensor-derived embryogenesis, the first morphologically distinct event is a wrong suspensor cell division. The daughter cells of the wrongly divided suspensor cell continue to proliferate and may form a second embryo-like structure. It has been shown that in phenotype *twin1* both the zygotic embryo and the suspensor-derived embryo can develop alongside each other, generating so-called 'twin' plants. A question that has remained unanswered is when during suspensor-derived embryogenesis suspensor cell lose their identity and embryo identity is acquired. To answer part of this question, when suspensor identity is lost, live-imaging of *Arabidopsis thaliana* ovules is done using suspensor-specific fluorescent markers. In live-imaging, *in-vitro* culturing of ovules is an essential part where the goal is to keep the ovules in favorable conditions for as long as possible. To enhance the conditions, an *in-vitro* culturing device using PDMS micropillars to fixate ovules is altered. A channel was cut in the walls of the device which enhances culturing medium flow which subsequently increased ovule survival rate. Continuing with live-imaging, fluorescent markers were previously transformed into two plant lines possessing a chance to express aberrant suspensor phenotypes, *twin1* and M0171>*bdl*. In these two models for observing suspensor cell fate loss, suspensor cell fate is estimated to be lost prior to wrong suspensor cell division(s) and definitively lost post wrong division in *twin1* while in M0171>*bdl* suspensor cell identity seems to remain in daughter cells of wrongly divided cells. To answer when during suspensor-derived embryogenesis embryo identity is acquired, a double marker line was selected with a suspensor-specific component driving expression of tandem-Tomato fluorescent protein and a proembryo-specific component driving expression of green fluorescent protein. Unfortunately, silencing of the proembryo-specific component occurred. However, with an eye on the future a technical problem with living-imaging double markers during twin embryogenesis was tackled. During live-imaging twin embryogenesis, GFP and tdTomato may be present within the same cell nucleus. Using root tips this was simulated and fluorescence bleed-through from GFP to tdTomato is observed. For live-imaging twin embryogenesis with double markers this implies that a bleed-through component has to be evaluated before an interpretation of changes in fluorescence intensity can be made.

Table of contents

Introduction

Embryogenesis in *A. Thaliana* normally starts by double fertilization of the zygote (Figure 1). After fertilization, the zygote divides asymmetrically into a large basal cell and a smaller apical cell (Figure 1). The apical cell continues to divide to form the proembryo, while the basal cell continues to divide horizontally to form the suspensor, which provides nutrients and growth factors to the growing embryo. The embryo passes several stages through embryogenesis to form the blueprint of the mature plant from a minimal number of cells (Berleth & Chatfield, 2002). Embryogenesis stages are marked by the number of proembryo cells or, later in embryogenesis, marked by the shape of the proembryo. Starting after the first cell division of the smaller apical cell, the 2-cell stage is reached, similarly, after another round of cell divisions, the 4-cell stage and subsequently the 8-cell stage or also known as octant stage are reached. Following more rounds of cell divisions, in the following order, dermatogen, globular and heart stage are formed. Both globular and heart stage can be further divided into early-, mid-, or late- stage. At the end of heart stage, early embryogenesis is complete. Additionally, at the end of heart stage the suspensor stops dividing and an eight-cell-long structure below the embryo is formed. At heart stage, cell patterning is complete and the blueprint of the mature plant has been established. Following heart stage, the previously established cell pattern is merely elaborated upon (Berleth & Chatfield, 2002; Smyth, 1990).

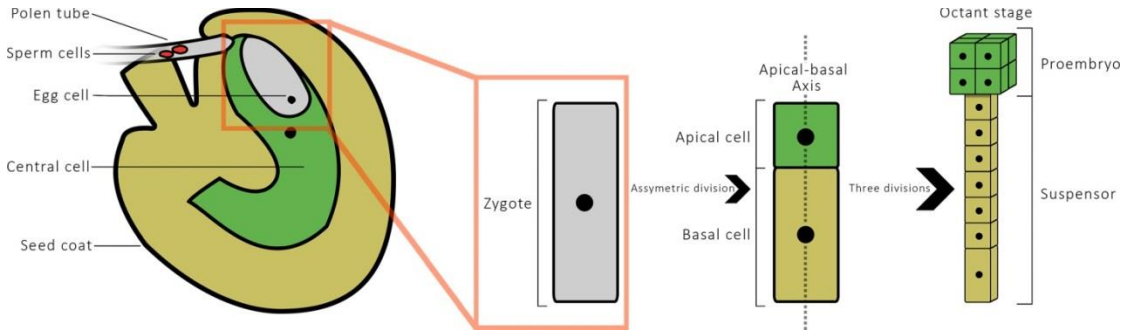

Figure 1: On the left: schematic representation of an ovule. On the right: schematic representation of a zygote dividing assymetrically into an apical cell and a larger basal cell and subsequent cell divisions that give rise to octant stage and the suspensor. The apical-basal axis is marked.

In addition to zygotic embryogenesis, plants possess the capability to derive embryos from somatic cells. Different routes have been proposed on how somatic cells end up with an embryo identity (Figure 3). Somatic cells may directly convert to an embryo-identity or first revert back to a pluripotent state before adopting an embryo identity (Srivastava & DeWitt, 2016). Additionally, installment of competence for the transition to embryo identity may be an additional requirement (Radoeva, 2016). To further complicate the matter, much is unknown about the initial factors required to initiate a transition to embryonic identity. In *A. thaliana* one type of somatic cells, the previously introduced suspensor cells, have been shown to able to form embryo-like structures that may eventually grow into full grown plants. In that case the zygotic embryo and suspensor-derived embryo grow alongside each other, generating so-called 'twins' (Radoeva, 2016; Vernon & Meinke, 1994). The first morphological distinct event during suspensor-derived embryogenesis is an extra cell division of one of the suspensor cells (Figure 2). Mostly, this extra division is a vertical division which in wild type suspensors does not appear.

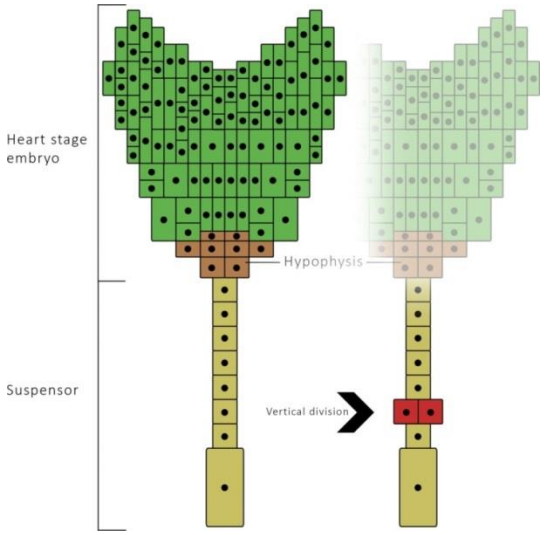

Figure 2: Schematic representation of a heart stage embryo with a vertical division at the seventh suspensor cell.

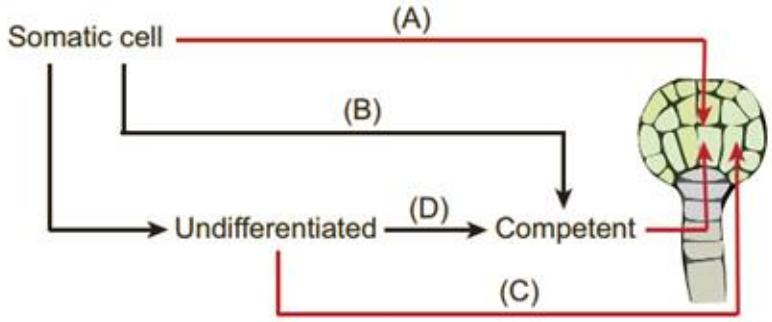

Figure 3: Four routes from somatic identity to embryo identity. (A) direct transdifferentiation. (B) instalment of competence followed by embryo identity specification. (C) de-differentiation, followed by embryo identity specification (D) de-differentiation followed by instalment of competence and embryo identity specification. Image and caption were taken from (Radoeva, 2016).

Previously, two phenotypes have been described, *twin1* and M0171>*bodenlos*, in which wrong divisions in suspensor cells are occur. *Twin1* is a pleotropic mutant that displays incomplete penetrance (8-31%) of a wide range of defects in embryonic cell division(s), morphological development and seedling growth. Most importantly, *twin1* has a twin phenotype penetrance of 9% and aberrant development has only been seen in embryos post early-globular stage (Vernon & Meinke, 1994). Aberrant development in the suspensor includes vertical divisions, irregular division planes and long suspensors containing more than eight suspensor cells.

M0171>*bodenlos* has an inducible phenotype with a penetrance of 31% in early embryogenesis up to 83% at heart stage (Rademacher et al., 2012). *Bodenlos (bdl)* is a stabilized mutant (of BDL). Although irrelevant here, BDL is normally expressed in proembryonic cells where it inhibits auxin response factor (ARF) 5, otherwise known as monopteros (MP). When auxin enters the proembryonic cells, auxin promotes BDL degradation, releasing inhibition of ARF5 (Dharmasiri et al., 2005). In turn, ARF5 promotes basal PIN1 localization, which, consequently generates an auxin efflux from the proembryo towards the suspensor (Friml et al., 2002). The generated auxin efflux has been shown to be essential for hypophysis specification (Rademacher et al., 2012). Wrong suspensor cell divisions are generated when *bdl* is ectopically expressed in suspensor cells during early embryogenesis, where *bdl* continually inhibits various ARFs. This inhibition of a large part of the auxin response causes suspensor proliferation (Rademacher et al., 2012). These proliferating suspensor cells have also been shown to gain embryonic identity (Rademacher et al., 2012). Ectopic *bdl* expression was achieved with the two component GAL/UAS system. In this system, enhancer trap line M0171>GAL4 is used. M0171 is a suspensor-specific promoter which drives GAL4 expression. When M0171>GAL4 is crossed with a plant line containing a UAS-*bdl* construct, GAL4 binds to UAS which allows *bdl* transcription (Figure 4).

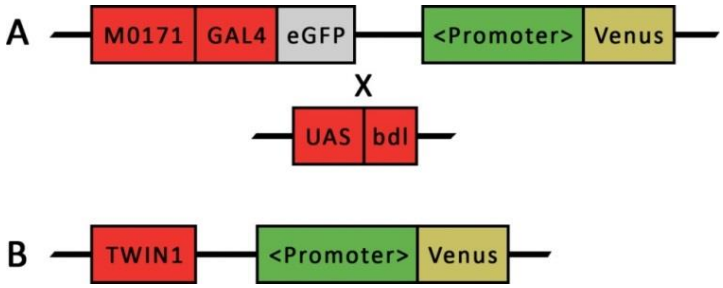

Figure 4: Schematic representation of genetic constructs in enhancer trap line M0171 and the pleotropic mutant *twin1*. The length of each block is not representative of actual gene length. Blocks that are connected are connected in the DNA. Whenever there is a break between blocks, blocks are located at different regions in the genome. In green are promoters that drive expression of a fluorescent protein, in this case Venus (yellow block). (A) M0171 crossed with a UAS-*bdl*. Additionally, the M0171 line also has a fluorescent marker construct (B) *twin1* and a fluorescent marker construct.

In *twin1* and M0171>*bdl*, the exact moment when suspensor cells lose suspensor identity and gain embryonic identity is unknown. To answer this question, here, live-imaging of cell-type-specific fluorescent markers is employed. Live-imaging requires care of living ovules. Luckily, previously, live-imaging has been developed where *A. thaliana* ovules were captured in polydimethylsiloxane micropillar devices(PMDs) and *in-vitro* cultured for up to 72h (Gooh et al., 2015). Here the PMD design is altered and its effect on ovule survival rate is determined.

Using *in-vitro* cultured ovules, the ovules were live-imaged with fluorescent markers. These markers were previously transformed into plant lines mediated by agrobacterium (Radoeva, 2016). The marker's transgene contains a promoter of a suspensor-specific or proembryo-specific gene. In turn, the promoter drives expression of a fluorescent protein.

Suspensor-specific promoters were used to identify when suspensor cell identity was lost in *twin1* and M0171>*bdl*, respectively. The promoters used were WRKY2 and ATPase. WRKY2 has been linked to suspensor identity whereas ATPase was identified during a screen for embryo inducers (Radoeva, 2016; Ueda, Zhang, & Laux, 2011a). To identify when embryo identity is acquired a double marker with a suspensor-specific component and a proembryo-specific component is tried to be used. The double marker has a suspensor-specific component with the Cobra-like 6 promoter (pCOBL6) and a proembryo-specific component with the promoter from DÖRNROSCHEN (pDRN). pCOBL6 drives expression of tandem-tomato (tdTomato) fluorescent protein and pDRN drives expression of green fluorescent protein (GFP). In live-imaging GFP and tdTomato may be in the vicinity of each other. Thus, GFP may activate tdTomato. This phenomenon is named bleed-through and, here, in addition to determining when suspensor cell identity is lost using suspensor-specific markers pATPase::Venus and pWRKY2::Venus in *twin1* and M0171>*bdl*, GFP to tdTomato bleed-through is simulated in *A. thaliana* root tips.

Material & Methods

Seed sterilization

A. thaliana seeds were sterilized for 10min in 75% ethanol/25% bleach solution. Subsequently, seeds were washed twice with 70% ethanol and once with 96% ethanol and allowed to dry in a flow cabinet for roughly 2h.

Seed plating

A bottle containing 400ml solid ½ Murashige and Skoog (MS) medium was heated in a microwave for 5min30s at 70% power. The MS medium was allowed to cool down until it was bearable to touch with hands. In some cases, depending on *A. thaliana* plant line used, an antibiotic marker was added (Table 1).

Table 1: Antibiotic markers used and their stock concentration in liquid MS medium.

Selection marker	**Concentration (mg/l)**
Norfloxacin	10
Phosphinotricin	15
Methotrexate	10

After heating and or adding an antibiotic marker, roughly 50ml liquid MS medium was poured in a 120mm square petri dish. Liquid MS Medium was allowed to solidify for roughly 30min. After solidification, sterilized *A. thaliana* seeds were sprinkled onto the plate and the plate was left overnight in a cold room (4°C). The next day, plates were transferred to a climate chamber (long day conditions, 16 hours light; 8 hours dark, at 22°C).

Planting seedlings

For *twin1* seedlings, roughly 7 days after growth on medium plates, seedlings were first selected based on whether they had a twin. Selected twins were then allowed to continue growth on a new medium plate for 3 to 5 days to recover from the selection procedure. After recovering, twin seedlings were placed on soil. For non-*twin1* seedlings, roughly 7 days after seeds germinated on medium plates, seedlings were placed onto soil. For both *twin1* and non-*twin1* seedlings, the soil tray was placed in the climate chamber (long day conditions, 16 hours light; 8 hours dark, at 22°C).

Plant screening

Previously, plasmids bearing fluorescent markers were introduced by floral dip. Plant lines with strong marker fluorescence were already selected for. However, some plant lines were still segregating the introduced marker construct. Therefore a screen for marker expressing plants is done.

Renaissance 2200 dye (Ren Dye) was prepared by adding 42 µl DMSO, 100 µl 50% glycerol, and 22µl Renaissance 2200 to 900µl paraformaldehyde (4%) in phosphate-buffered saline (1%). 3-5 siliques, secured to tape, were cut open through their replum under a binocular using a 0.6x25mm dissecting needle (Figure 5A-B). All ovules were transferred from the cut open silique to a drop of Ren Dye on a microscope slide. A 24x50mm cover glass was placed on top of the Ren Dye droplet with ovules. Subsequently, embryos were popped out of ovules using a (2½ HB) pencil's point by gently tapping, close to ovules, on the cover slip.

Leica's SP5 scanning confocal microscope was used in conjunction with a 20x water-immersion objective and a 63x water-immersion objective. The 20x water-immersion objective was used for screening through the prepared sample using bright field (BF) while the 63x water-immersion objective was used for imaging of popped embryos. Leica's LAS AF software was used to obtain images. In LAS AF, Image acquisition settings used are shown in (Table 2).

Table 2: LAS AF acquisition settings for Ren Dye, GFP, Venus and tdTomato.

FP	Laser	Exc.λ (nm)	Em. λ (nm)	Mirror
Ren dye	Diode	405	430-460	RT30/70
GFP	Argon	488	500-535	RSP500
Venus	Argon	514	550-600	DD458/514
tdTomato	Argon	554	560-590	DD488/561

Live-imaging

The entire live-imaging procedure including preparations was done aseptically to exclude microorganism contamination. 10ml Live imaging-medium was prepared using 5ml MQ, 2ml trehalose (25% w/v), 1ml MES-KOH

(0.5% w/v), 1ml Vitamin B5 (0.112% w/v), and 1ml Nitsch salts (2.2% w/v) (ratio 5:2:1:1:1). Siliques from plants were carefully selected to ensure that ovules in early embryogenesis stages were selected. 3-5 siliques were cut open aseptically similar to the procedure in *Plant screening* (Figure 5A-B). Next, ovules were transferred one-by-one to a drop of live-medium on top of a PMD (Figure 5B-C). The live-medium drop was warped to fit the PMD's inner area (Figure 5D). Next, live-medium was removed so that the drop was flat rather than round (Figure 5E; Figure 6). The PMD was flipped up-side-down inside a chamber of an imaging device (Figure 5E-F). Subsequently, the imaging chamber was filled with live-medium until the PMD was submerged (Figure 5G).

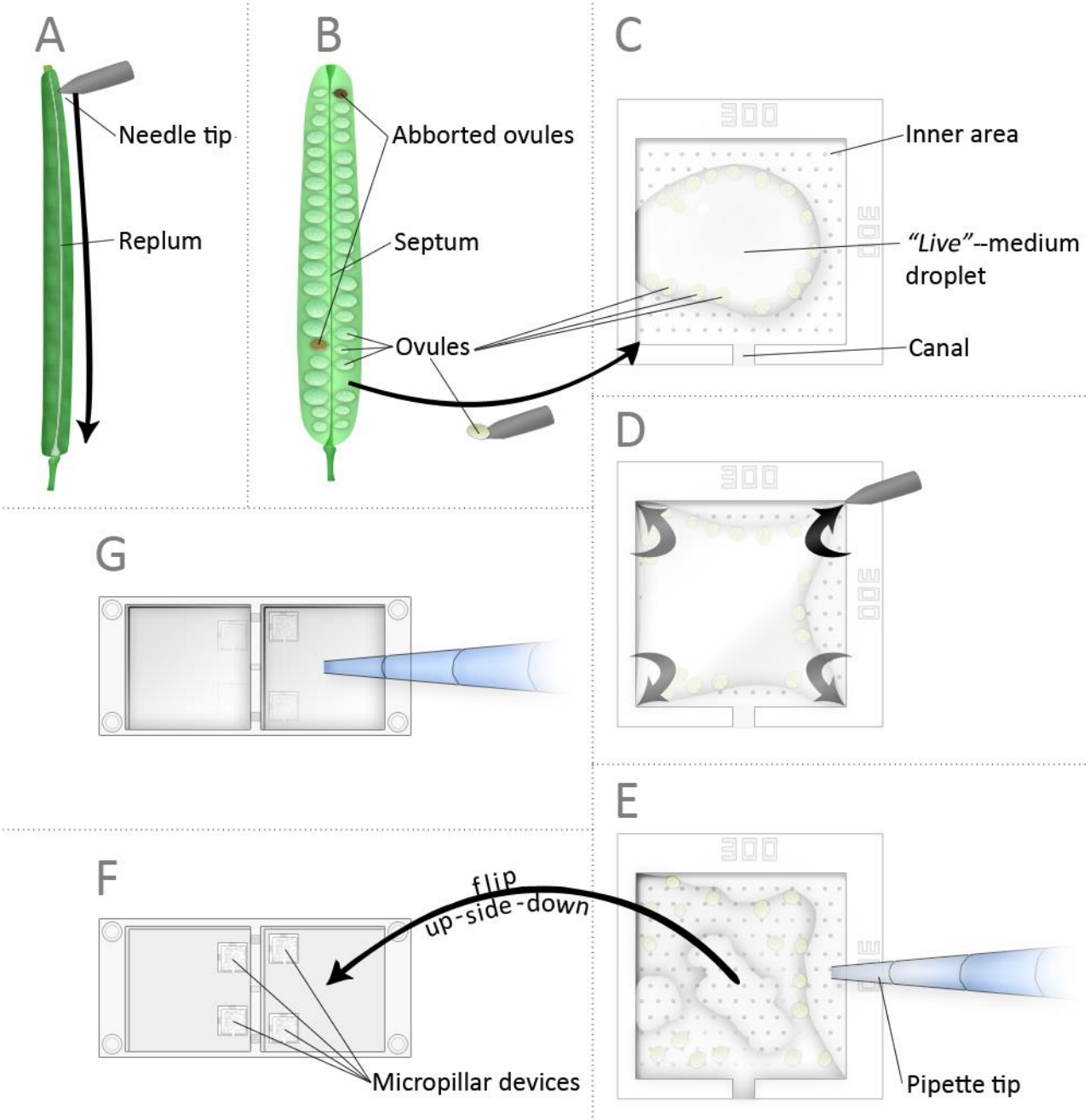

Figure 5: Live-imaging preparation of PMD in imaging chamber. (A) Cutting open *A. thaliana* silique. (B) Opened *A. thaliana* silique, selecting white and transparent ovules, and transferring ovules to PMD. (C) PMD with LMD. Channel allows live-medium flow in and out of PMD. (D) Warping LMD to edges of PMD. (E) Removing live-medium to flatten bulging LMD. Flipping PMD up-side-down into imaging chamber. (F) Imaging device containing four PMDs, two PMDs per imaging chamber. (G) Filling imaging chambers with live-medium until PMDs are completely submerged.

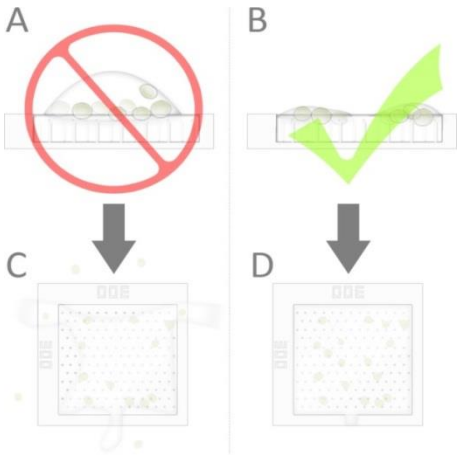

Figure 6: Live-medium droplet on PMD. (A) Bulging live-medium droplet. (B) flat live-medium droplet. (C-D) Results of A or B when PMD is flipped up-side-down inside imaging chamber.

For live-imaging, Leica's SP8 inverted laser scanning confocal microscope was used in conjunction with a white light laser (WLL) at 50% power. Here, the WLL penetrates the ovule from below to reach suspensor cells and excite the fluorescent marker in nuclei of suspensor cells. Emitted fluorescence then travels a similar path through various cell layers in order to reach the detector while out-of-focus light is blocked by a pinhole set at 1 Airy (60.7µm) (Figure 7).

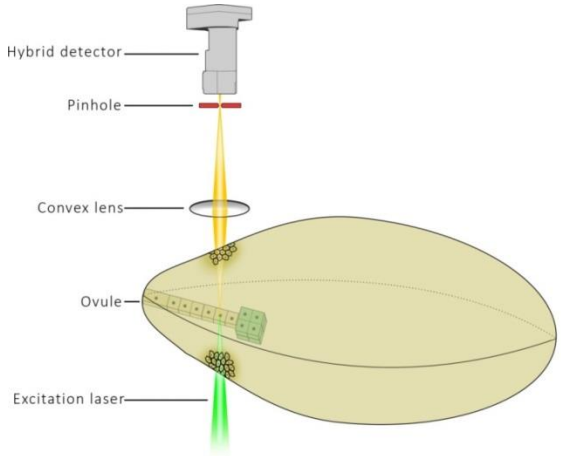

Figure 7: Schematic representation of confocal microscopy. An excitation laser penetrates the seed coat of an ovule to excite fluorescent proteins in a suspensor cell. Emission light passes through a convex lens and at full convergence emission light passes through a pinhole to reach a hybrid detector. It should be noted that in the image emission light travels upwards, while in Leica's SP8 inverted laser scanning confocal microscope setup, emission light travels downwards towards to the same direction the excitation laser originated from to reach the Hybrid detector.

To obtain images of captured fluorescence Leica's LAS X software was used. After preparing PMDs inside an imaging device, the imaging device was locked onto the microscope's motorized stage. An 20x glycerol (20%) immersion objective was used for both BF microscopy and live-imaging. Ovules for live-imaging were either selected manually by screening through the prepared sample using BF microscopy or a tilescan was made of the PMD's inner area to localize ovules with fluorescent signal (Figure 8).

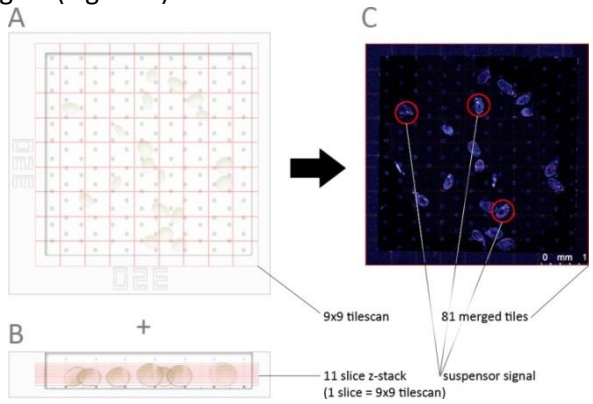

Figure 8: (Graphical) representation of tilescan. (A) up-side-down PMD, in red 81 tiles. (B) PMD side-view, in red 11 z-stack slices. (C) Image acquired from tilescan, all 81 tiles are merged. In red 3 suspensor signals are imaged.

A custom z-stack was generated for each selected ovule. The z-stack included the entire z-range in which fluorescent marker signal was observed (Figure 9). Because it was observed that ovules move roughly 30 µm downwards in the first 6-20h, an additional 30µm was added to the z-stack margin in the downward direction. Z-step size was set at 10µm or 5µm depending on time required to image all ovules and clarity of fluorescent signal. When the time required to image all ovules was below one hour, a consideration was made to decrease z-step size from 10µm to 5µm when an ovule showed clear fluorescent signal in all suspensor cells. This consideration was made purely based on curiosity to view whether decreasing z-step size had any effect on how fluorescent signal in suspensor cell nuclei was viewed.

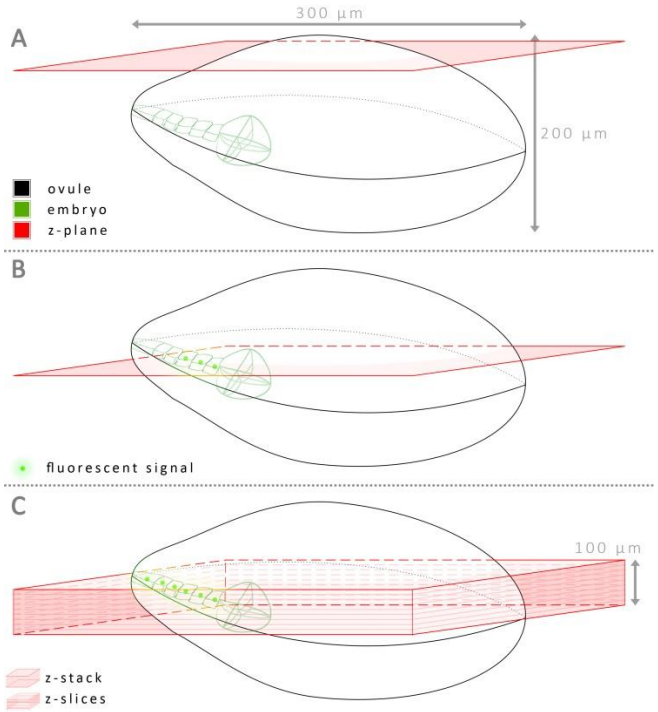

Figure 9: Instructional image for generating a z-stack. (A) z-plane is located above the suspensor. (B) z-plane is aligned with the suspensor and a fluorescent signal emitted from suspensor cells should now be visible. (C) A z-stack 100µm in size, consisting of roughly 10 z-slices. Dimensions shown are rough averages observed during live-imaging ovules.

With each ovule having a custom z-stack, ovule positions were sequentially imaged for 12-110h with an imaging interval of 1h. Leica's hybrid detector was used with image acquisition settings shown in (Table 3). Additionally, scanning speed was set at 400Hz, scan direction was unidirectional or bidirectional (X-phase 32.14), an image resolution of 1024x1024 was used, a zoom factor of 1x – 3x was used and line averaging was set to 8x. Finally, gain was adjusted to ovule locations that had the most promising signal to ensure that the fluorescent proteins were neither over-/ or underexposed.

Table 3: LAS X, WLL, acquisition settings for GFP, Venus and tdTomato.

FP	**Excitation λ (nm)**	**Emission λ (nm)**	**Power (%)**
GFP	480	500-535	50
Venus	514	535-560	35
tdTomato	554	560-590	50

In some over-the-weekend live imaging experiments, live-imaging was stopped mid-way to adjust ovule position and deselect ovules with no signal. This was done to generate extra imaging time for ovules that did show good suspensor signal. Thus, for ovules with good signal, z-step size and imaging interval was decreased, and zoom and imaging resolution may have been increased.

After completion of live-imaging, z-stacks are searched for z-slices in which the fluorescent signal emitted from suspensor cell nuclei is sharpest. Sometimes suspensors where visible in one z-slice, other times, the signal from suspensor cell nuclei was scattered over multiple z-slices. In the latter situation, a maximum projection of all the z-slices with fluorescence from suspensor cell nuclei was made.

Results

Alteration of PMD to increase ovule survivability

In live-imaging ovules are *in-vitro* cultured to mimic the environmental conditions ovules naturally reside in. The goal of *in-vitro* culturing here is to extend the ovule lifetime as long as possible. In turn, a long ovule lifetime corresponds with a long time that fluorescent signal can be imaged. Therefore, *in-vitro* culturing of ovules is essential for live-imaging. During preparations of PMDs with ovules it was observed that live-medium did not flow into the inner area of the PMD (Figure 11A-D). It was suggested that due to the lack of medium flow and the fact that some ovules were not surrounded with live-medium, the ovule survival rate was not at its maximum potential. In an effort to increase the ovule survival rate the PMD's design is altered to enhance live-medium flow, and subsequently, the effect of the new PMD design on ovule survival rate is tested.

The alteration introduced to the PMD design is visually represented below (Figure 10). A channel was cut into the walls of the PMD to allow live-medium flow from outside of the PMD to inside of the PMD. Live-medium flow from outside to inside is indeed observed over time (Figure 11E-G). Additionally, it was observed that ovules in channelled PMDs could stay alive for a 330 hours (and potentially longer). From this observation it was expected that live-medium flow enhanced ovule survival rate. However, it was unsure whether channelled PMDs enhance ovule survival rate because in one instance ovules remained alive for 144 hours in non-channelled PMDs (Figure 11D).

Figure 10: Illustration of a non-channelled PMD and channelled PMD. (On the left) PMD without a channel in which medium does not spread evenly across the PMD's inner area. (On the right) Visual illustration of where a channel was cut in the walls of PMDs.

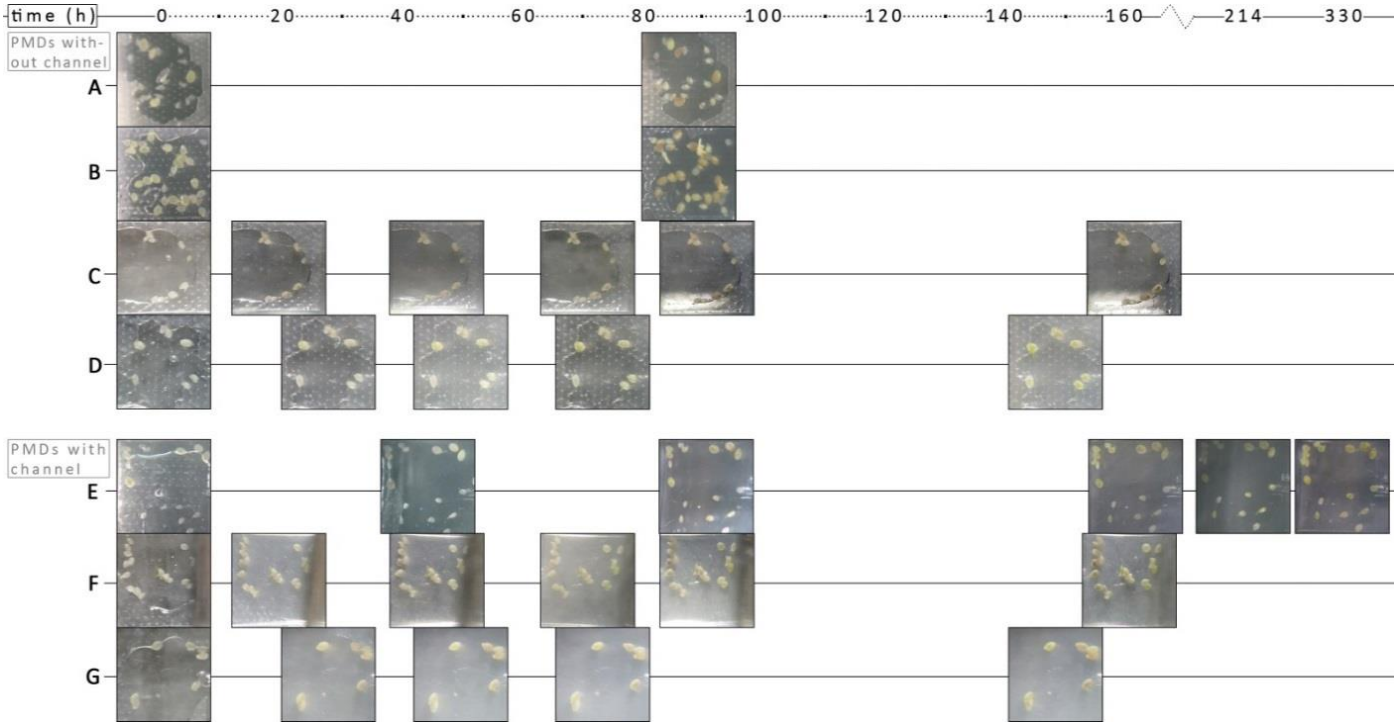

Figure 11: Ovules inside PMD's inner areas at various time points throughout *in-vitro* culturing. (A-C) PMD's without a channel. (D-G) PMDs without a channel. (H-I) PMDs without a channel and PMD was not submerged in live-medium. Pictures were taking with a SONY XPERIA XA camera through the ocular of a binocular. Developmental stages of embryos in D and G can be found in supplemental information (Figure S1).

To test whether ovule survival rate is indeed increased in channelled PMDs, an ovule death rate (ODR) is determined in 9 non-channelled PMDs and 7 channelled PMDs. This ODR is the amount of dead ovules over the total amount of living ovules present at the start of live-imaging. Ovule survival was assessed by ovule colour, ovules that are translucent or ovules that turned green were assessed as living, while, ovules that turned brown were assessed as dead (Park, Kurihara, Higashiyama, & Arata, 2014). However, although irrelevant in this chapter, it should be noted that in live-imaging, brown coloured ovules can sometimes still show marker expression. For non-channelled PMDs,

the ODR was determined after 62-69h of live-imaging while for channelled PMDs, the ODR was determined after 67-69h of live-imaging (Figure 12). From the ODR, the ovule survival rate (OSR) was determined with (Equation 1).

$$OSR = 1 - ODR$$

Equation 1: Ovule survival rate (OSR) is determined from ovule death rate (ODR). With the rate of death ovules known, the other half of the ratio is simply the half of living ovules. This is seen in this equation by subtracting ODR from '1'.

For non-channelled PMDs the OSR is 0.42 while for channelled PMDs the OSR is 0.71. Comparing both OSRs shows that ovule survival in channelled PMDs is 1.7 times higher in channelled PMDs than in non-channelled PMDs when ovules are live-imaged for 62-69h.

It is expected that the increase in ovule survival as a result of enhanced medium flow is caused by an increased influx of nutrients towards ovules and an increased efflux of (toxic) waste products away from ovules. Additionally, it was previously suggested that trehalose confers enhanced tolerance to stresses induced by *in-vitro* culturing conditions (Gooh et al., 2015). An increased influx of trehalose towards ovules may enhance trehalose's effect on ovules.

Ovule growth characterization

In an effort to further enhance *in-vitro* culturing, ovule growth is characterized in PMDs. This is done by measuring ovule growth in major and minor axis (Figure S1). Growth is measured for 66 ovules at the start (t=0h) and end of live-imaging (t=45 – 88h) (Figure 13).

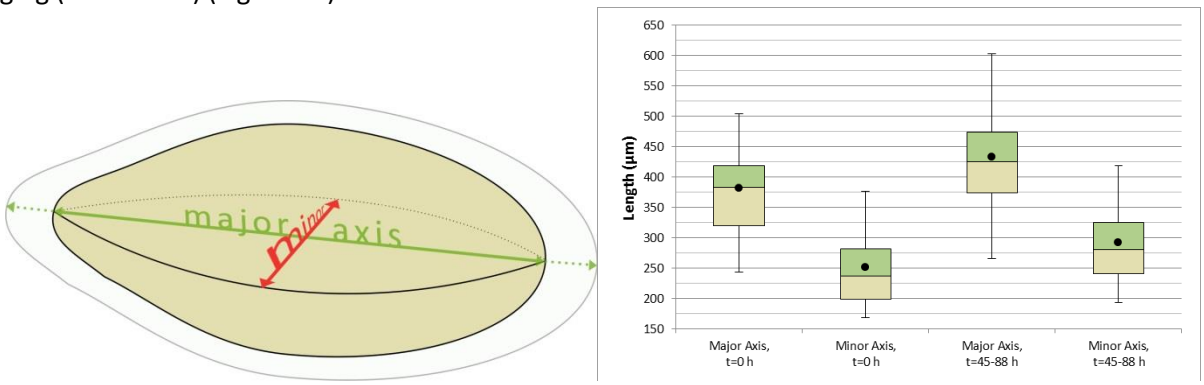

Figure 13: On the left, graphical representation of an ovule, indicating major and minor axis and growth. The use of major and minor axis was replicated from (Park et al., 2014). On the right, boxplot of major and minor axes lengths at 0 hours and after 45-88 hours of 66 ovules. Black dots are averages.

On average, at the start of live-imaging, ovules are 382µm and 245µm long in the major axis and minor axis, respectively. During 45-84 hours of live-imaging, ovules, on average, grow up to 430µm and 289µm in major axis and minor axis, respectively (Figure 13).

Next to knowing how big ovules grow and observing how ovules grow aberrantly sometimes (Movie S3), nothing is done with ovule growth to enhance live-imaging, for now. However, in the discussion ovule growth in PMDs will be compared to ovule growth in flexible PDMS cages.

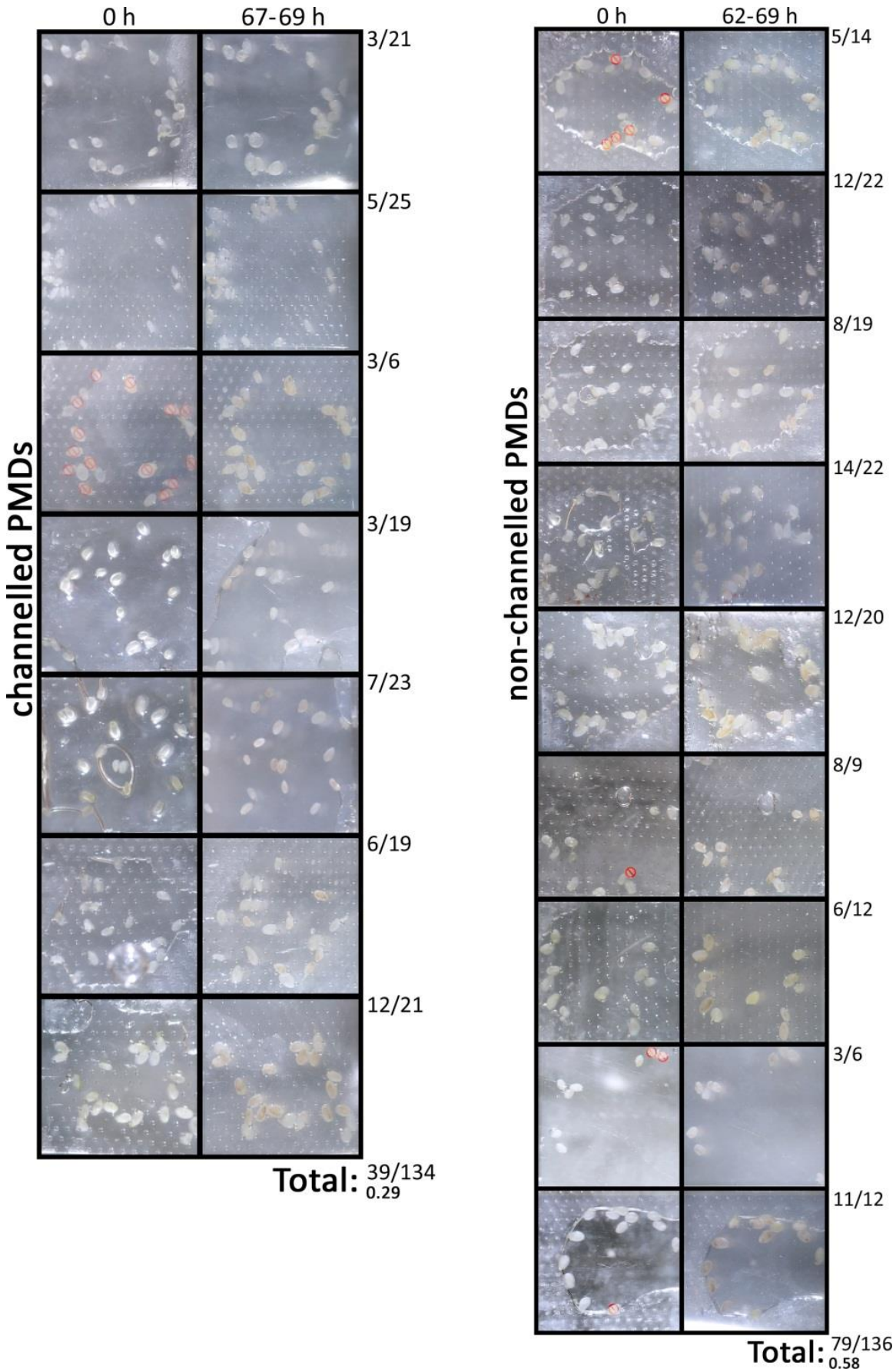

Figure 12: Non-channelled and channelled PMDs with ovules inside PMD's inner area at t=0 and t=62-69h of live-imaging. Next to each PMD combination there is an ovule viability ratio. This ovule viability ratio is summed and averaged over non-channelled and channelled PMDs at the bottom. Ovules with a red cross are not included in ovule viability ratios.

(live-)imaging fluorescent markers in A. thaliana ovules

In the introduction an question was introduced when during suspensor-derived embryogenesis suspensor identity is lost and embryo identity is acquired. To partly answer this question, when during suspensor-derived embryogenesis suspensor cell identity is lost, developing *twin1* and M0171>*bdl* ovules are live-imaged with suspensor-specificensor-specific fluorescent markers, pATPase::Venus and pWRKY2::Venus. However, first, a short description of the function of each promoter in the marker constructs is given as well as the expression pattern of each marker in wild type. Also, for live-imaging, strong fluorescent markers are a requirement to be able to visualize the suspensor. Therefore, the fluorescent signal strength from each marker is tested in live ovules. Next to a strong fluorescent signal, the signal has to be present for a prolonged time to capture as many rounds of cell divisions as possible. Thus, the potential time marker signal is retained in live ovules is observed. Lastly and finally, pATPase::Venus and pWRKY2::Venus activity is observed and discussed in *twin1* and M0171>*bdl*.

Both promoters WRKY2 and pATPase have a suspensor-specific expression pattern (Figure 14A-B). However, only the function of WRKY2 has been well-described so far. WRKY2's activity will not be described in detail; instead all that will be mentioned is: WRKY2 directly regulates WOX8, WOX9 and non-cell autonomously regulates WOX2. WRKY2 can be said to be linked to maintaining suspensor identity because in *wrky*2 mutants secondary embryo-like structures were formed derived from the uppermost suspensor cell(s) around globular stage (Ueda, Zhang, & Laux, 2011b). WRKY2's expression pattern overlaps with WOX8's expression pattern and is restricted to suspensor cells (Figure 14B).

In contrast to WRKY2, pATPase's function is not known yet. pATPase was during a screen for embryo inducers and all that is known is that the ATPase gene encodes an ATPase that is localized in the mitochondria (Radoeva, 2016). Although it was already known that pATPase's activity is restricted to the suspensor cells, pATPase's expression pattern was, again observed coincidentally with plant screening of *twin1* plants. This was done in fixated embryos up to heart stage with fluorescent marker construct pATPase::Venus (Figure 14A).

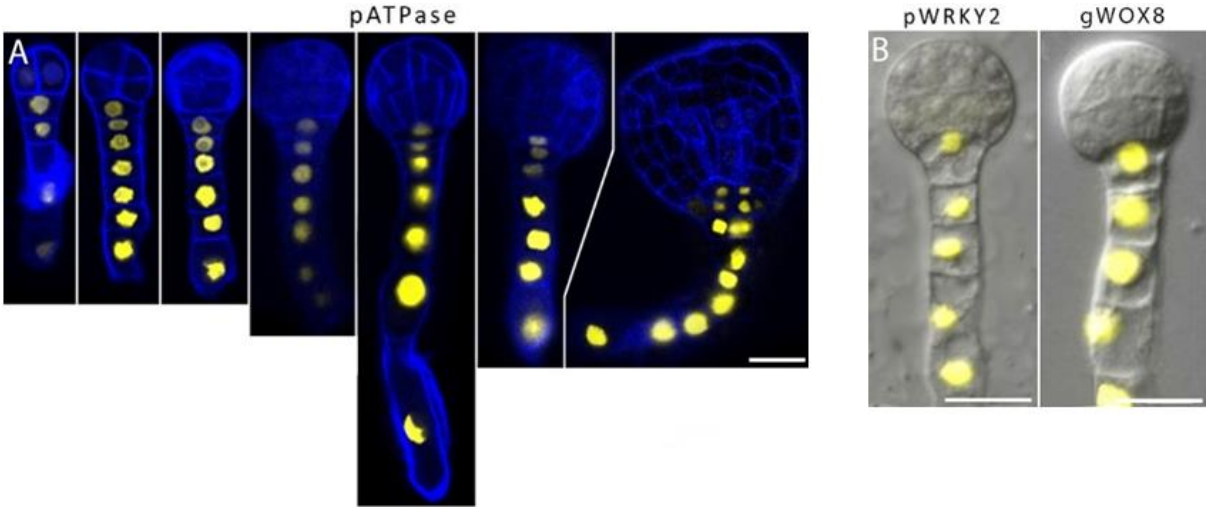

Figure 14: Expression patterns of pATPase>Venus and pWRKY2>Venus in wild type. For pATPase, from left to right embryos are put in chronological order of embryogenesis. The last embryo at late globular stage may have an aberrant division of the hypohysis. Scale bar (bottom right) is 20µm. pWRKY2's image is taken from (Ueda et al., 2011b).

pATPase expression pattern is, like expected, restricted to the suspensor (Figure 14A). However, regularly it was observed that around heart stage pATPase activity is extended to the columella and the hypophysis. However, this was not seen consistently and because the embryos used were obtained from a plant line containing the *twin1* gene, the extension of pATPase's activity to columella and hypophysis could be attributed to an aberrant phenotype.

Next, fluorescent signal generated by pATPase::Venus and pWRKY2::Venus has to be strong enough to be able to penetrate through multiple cell layers, including the seed coat, to reach the detector. In other words, both promoters have to have a high activity to generate a large abundance of fluorescent proteins. To test whether this was the case, it was simply checked whether Venus's fluorescence emitting from suspensor cell nuclei was visible in live ovules. Fortunately, both pATPase::Venus and pWRKY2::Venus were both clearly visible in live ovules and thus both markers suffice for live-imaging (Figure 15).

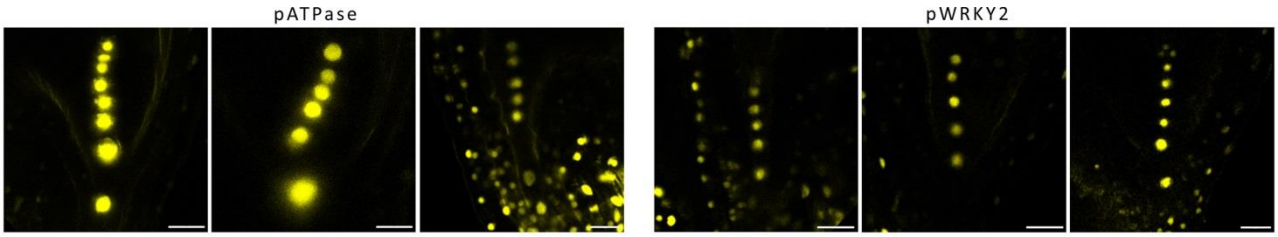

Figure 15: pATPase::Venus and pWRKY2::Venus in live ovules of DW bearing *twin1* and M0171, respectively.

In addition to a strong fluorescent marker, a second requirement in live-imaging is for the marker to be active for a prolonged time. This is, self-evidently, to observe marker activity for a prolonged time. To test how long marker signal is maintained in *in-vitro* cultured ovules, the presence of fluorescent marker signal was checked at the start of *in-vitro* culturing and after 110 hours. This was done for eighteen ovules. Additionally, it should be noted that in the first 64 hours the ovules were live-imaged. Thus, ovules were excited at 514nm for roughly three minutes every hour during live-imaging. Although it is unlikely, the excitation laser may have affected ovule viability (Waldchen, Lehmann, Klein, Van De Linde, & Sauer, 2015). After the first 64 hours of live-imaging ovules were stored at room temperature and *in-vitro* culturing was continued for the remaining 56 hours.

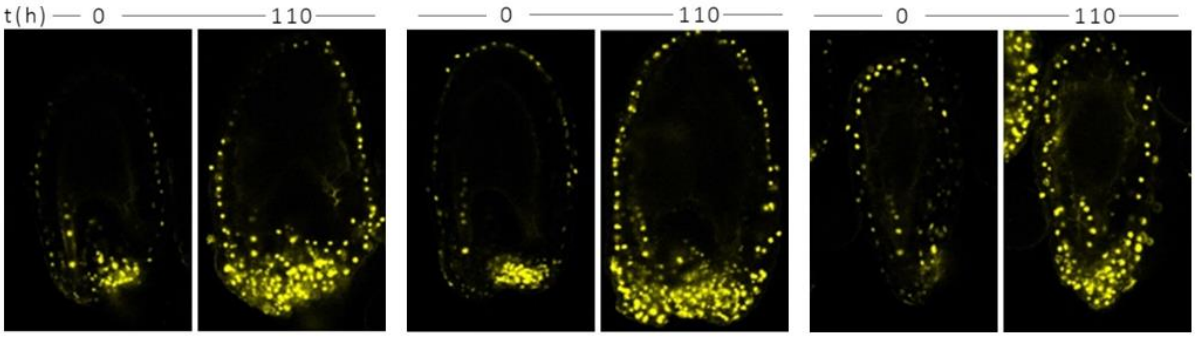

Figure 16: Three examples of pWRKY2::Venus in M0171 activity for 110h.

After 110 hours, all ovules remained alive. This was indicated by autofluorescence of the ovule's integuments. However, out of the eighteen ovules, only twelve ovules retained their marker signal (three examples shown in Figure 16). 110 hours of marker signal retention is an impressive amount of time because it was expected that ovules would only remain alive for 72 hours (Gooh et al., 2015). 110 hours of signal retention and potentially longer, illustrates the potential of live-imaging embryogenesis with fluorescent markers. The loss of signal in the other six ovules may be attributed to suspensor repositioning during development, which made the suspensor inaccessibile to be visualized with confocal microscopy; or the suspensor may have died around torpedo stage which is seen regularly; or, simply, the ovules had died.

Finally, knowing that pATPase::Venus and pWRKY2::Venus are viable markers for live-imaging and the potential of live-imaging has been illustrated, now, both marker's activity is discussed in phenotypes *twin1* and M0171>*bdl*. pATPase::Venus was previously transformed into *twin1* plants and pWRKY2::Venus was previously transformed into M0171. First, a wild type cell division is observed to illustrate how a normal cell division is observed when live-imaging suspensor cell nuclei. This may be used for comparison to wrong division(s) in *twin1* and M0171>*bdl*.

In wild type divisions, fluorescent signal intensity remains the same before and after cell division (Figure 17A, 0:00 – 1:04). In other words, the fluorescent signal intensity in the two daughter cells is equal to the fluorescent signal intensity in the mother cell. However, fluorescent signal size (or radius) is smaller in the two daughter cells compared to fluorescent signal size of the mother cell. The smaller signal size may be attributed to a smaller cell size of each daughter cell which is seen more commonly in the uppermost suspensor cells (Figure 14A). After cell division, fluorescent signal intensity remains constant for roughly 14h until the next cell division (Figure 17A, 1:04 – 15:41). The suspensor cell cycle is estimated to be around fifteen to eighteen hours (Figure S2). Because Venus's half-life is roughly 24 hours, from this can be concluded that after cell division pATPase is still active in both daughter cells because no decrease in signal intensity is seen which would be expected during this time.

Contrarily, it is proposed that when pATPase activity is actually shut down post division, fluorescent signal intensity will be halved in the two daughter cells. This proposition can be explained by the fact that when promoter activity is shut off, fluorescent protein that was produced before shut-off will still be present until degraded. Like previously mentioned the half-life of Venus is roughly 24 hours. Thus roughly 12 hours after shut-off, half of Venus fluorescent

protein will be degraded. However, shut-off can be visualized earlier when a division occurs. When a division occurs it is expected that the amount of fluorescent protein will be split over the two daughter cells and with that the fluorescent signal intensity will be split in half too. Because ATPase activity is linked to maintenance of suspensor identity, this way a definitive answer can be given to the question whether suspensor cell identity is lost post division. For the other marker pWRKY2::Venus, the same behaviour is expected.

In pWRKY2::Venus in M0171>*bdl*, multiple cell divisions are seen (Figure 17B & F). Both horizontal and vertical cell divisions are seen. In wild type, vertical divisions have never been seen. Therefore, these vertical divisions can be seen as 'wrong' divisions. In M0171>*bdl*, in most vertical cell divisions, it appears that fluorescent signal intensity decreases and later increases (Figure 17B, 00:00 – 18:46). However, when observing fluorescent signal intensity in neighbouring suspensor cells, the same pattern of first a decrease in signal intensity followed by an increase in signal intensity is seen. Therefore, it is expected that the whole suspensor is first less readily available to be visualised followed by being more readily available to be visualized. Thus, fluorescent signal intensities may change post vertical division; However, a definite change in fluorescent signal intensity cannot be observed. Because fluorescent signal is still present and does not seem to fade it is expected that WRKY2 is still active post vertical division. With that, it is expected that suspensor identity is maintained post vertical division. Only once does signal completely vanishes post vertical division in the top-most suspensor cell (Figure 17B, 4:31 – 31:16). Because in this instance fluorescent signal is retained in the rest of the suspensor cells, unlike the previous observation where the entire signal in all suspensor cell nuclei fades, it can be said that suspensor cell identity is lost in these top-most cells. Approaching the end of each time-lapse, fluorescent signal fades in all suspensor cell nuclei. This may be attributed to suspensors repositioning themselves within the ovule, or suspensors entering necrosis around torpedo stage, or simply the ovule dying as a result of the uncomfortable *in-vitro* culturing conditions (Yeung, 1993). From this can be concluded that there are mixed observations and that it seems that suspensor cell identity is, in most cases, not lost following a wrong division in M0171>*bdl*.

For pATPase::Venus in *twin1*, three time-lapses are discussed (Figure 17B, D and E). Contrary to M0171>*bdl*, the suspensors seem to be more stable with less fluctuation in fluorescent signal intensity in suspensor cell nuclei throughout the time-lapse. Again, in contrast to M0171>*bdl*, in *twin1*, fluorescence intensity decrease is seen before vertical division too (Figure 17D, 14:56 - 39:28, in one descendant of suspensor cell 4 and in all descendants of suspensor cell 5). Based on Venus's half-life (roughly 24 hours), this indicates a loss of suspensor identity an undetermined time before the decrease in fluorescence intensity. Next to this unique observation in *twin1*, fluorescent signal intensity decreases post vertical division(s) (Figure 17D, 14:46 - 23:28 & 34:08 - 56:32; Figure 17E, 14:08 - 18:50). This concludes that suspensor cell identity is lost post vertical division and possibly prior to wrong division. Loss of fluorescent signal intensity and with that loss of suspensor identity is a common observation in fixated *twin1* embryos too (Figure 18). Continuing with the time-lapse, in another instance, it appears that only one daughter cell loses suspensor identity post vertical division (Figure 17C). However, in the same instance, it appears that suspensor cells move on top of each other. This observation confirms that in aberrant phenotypes division planes are odd compared to wild type and can generate complex cellular structures.

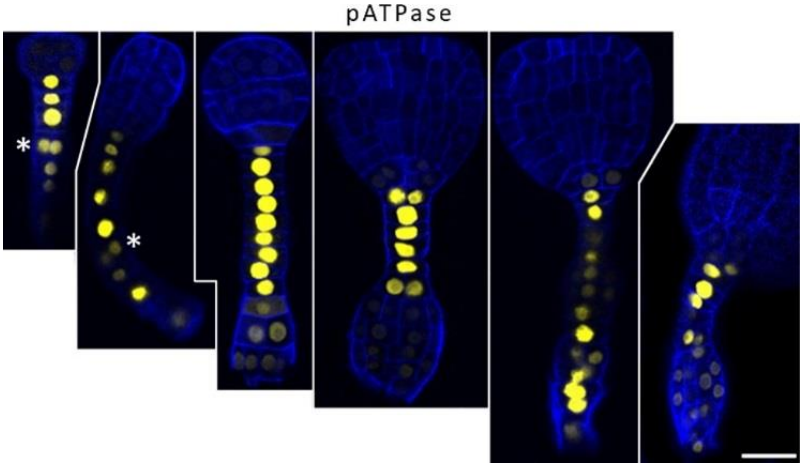

Figure 18: pATPase::Venus in embryos with *twin1* penetrance. From left to right embryos are put in chronological order of embryogenesis.

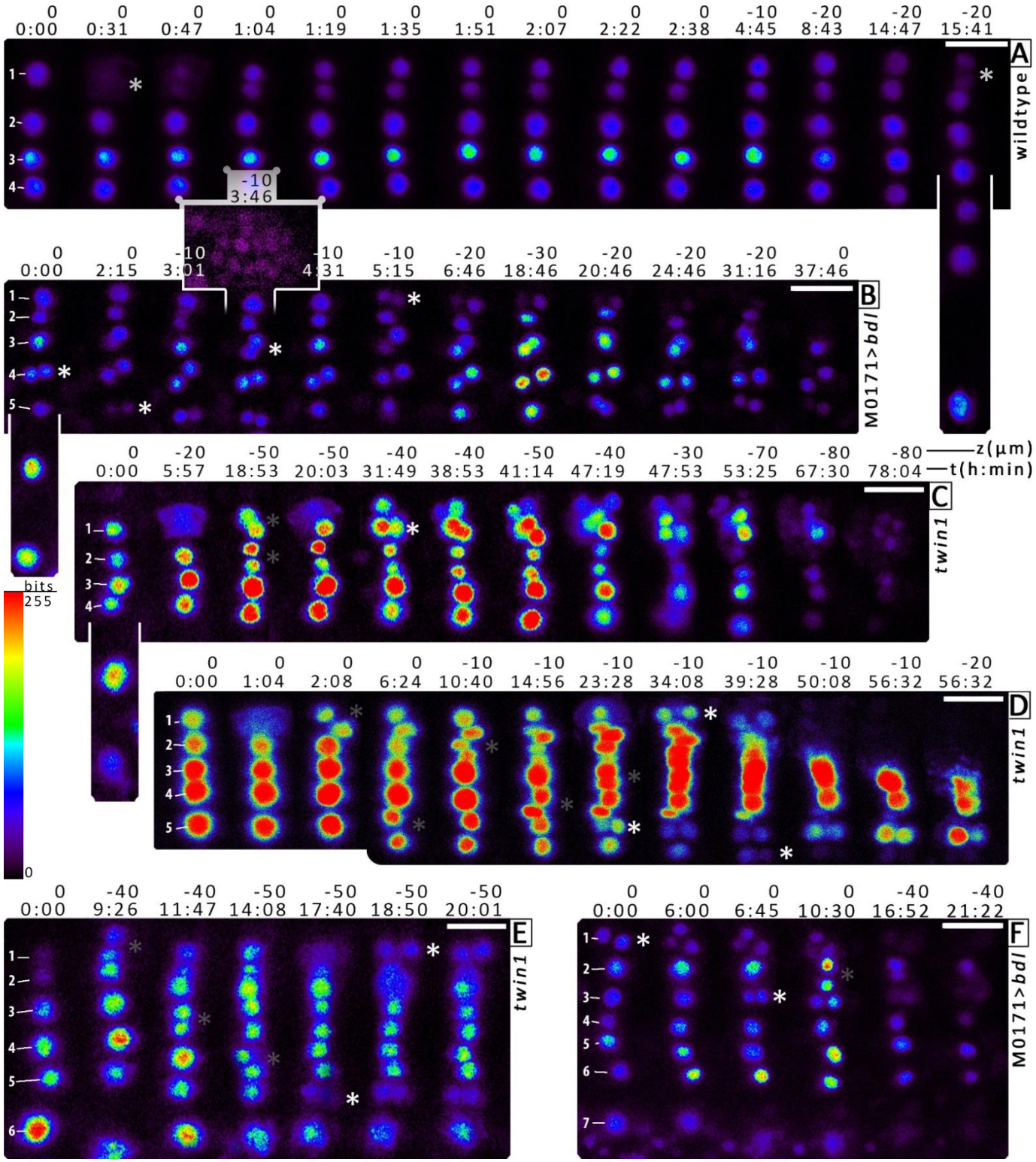

Figure 17: Seven series of snapshots taken from seven time lapses (A-F). (A) wild type suspensor cell division. (B and E) aberrant suspensor divisions caused by M0171>*bdl*. (C, D and F) aberrant suspensor divisions caused by *twin1*. Horizontal divisions are indicated with a gray asterisk (*) and vertical divisions are indicated with a white asterisk (*). White scale bars (top left) are 20 µm. An explanation for the creation of the snapshot series follows. Each snapshot was taken at a point in time when a change in suspensor cell number or a change in fluorescence intensity occurred. Additionally, the z-slice in which fluorescence intensity was highest was taken for each snapshot. For (B-E) each snapshot represents a single z-slice, whereas snapshots in (A) and (F) are maximum projections of two or more z-slices. The given z-position are relative to the first z-slice or first maximum projection. For snapshot series (A-C) the two most basal suspensor cells are only shown in one snapshot to show their existence and not wrongly depict *A. thaliana's* suspensor. However, no fluorescence intensity change or divisions of these two basal cells are seen and thus excluded in all other snapshots for their lack or relevance in these snapshot series.

Efforts to use double marker line for live-imaging

Initially the aim of this thesis was to not only determine when suspensor identity was lost but also to determine when embryo identity is acquired during suspensor-derived embryogenesis. To answer this two-part question a double fluorescent marker, pDÖRNROSCHEN::GFP-pCOBRA-LIKE6::tdTomato, that was previously generated could be used. pCOBL6 has specific activity in suspensor cells whereas pDRN has specific activity in proembryo cells. However, this implies that when proembryo identity is acquired while suspensor identity is not completely lost, GFP and tdTomato will be present within the same cell nucleus. GFP's emission spectrum overlaps with tdTomato's excitation spectrum (Figure 20). Thus, in theory, GFP could excite tdTomato. This phenomenon is named bleed-through. To test if GFP to tdTomato bleed through can occur during (live-)imaging, root tips are used to test this because it was easier. Two root tips are put next to each other, one root tip was derived from a plant previously transformed with an IAA33::GFP construct while the other root tip used was derived from a plant previously transformed with an IAA33:tdTomato construct. Both IAA33::GFP and IAA33::tdTomato's activity is seen in the root tip (Figure 21). However, GFP's fluorescence appears higher. This may be explained by GFP having a higher quantum yield than tdTomato.

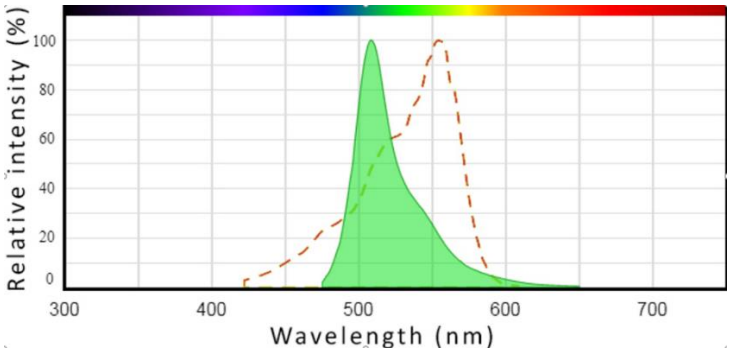

Figure 20: GFP's emission spectrum (green) and tdTomato's excitation spectrum (red).

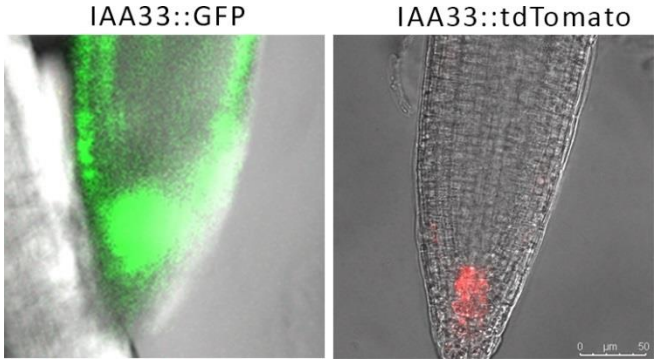

Figure 21: IAA33::GFP's and IAA33::tdTomato's expression patterns.

When only exciting GFP and imaging at GFP's emission range, only the IAA33::GFP root tip lights up (Figure 22A). This shows that GFP works and the root tip containing the IAA33::tdTomato construct can be used for comparison later, when tdTomato is excited. When exciting both GFP and tdTomato and imaging at tdTomato's emission range, there is slight GFP fluorescence and tdTomato lights up (Figure 22B). When only exciting GFP, and again, imaging at tdTomato's emission range, there is again slight GFP fluorescence and there is tdTomato fluorescence but less compared to when tdTomato was also excited (Figure 22C).

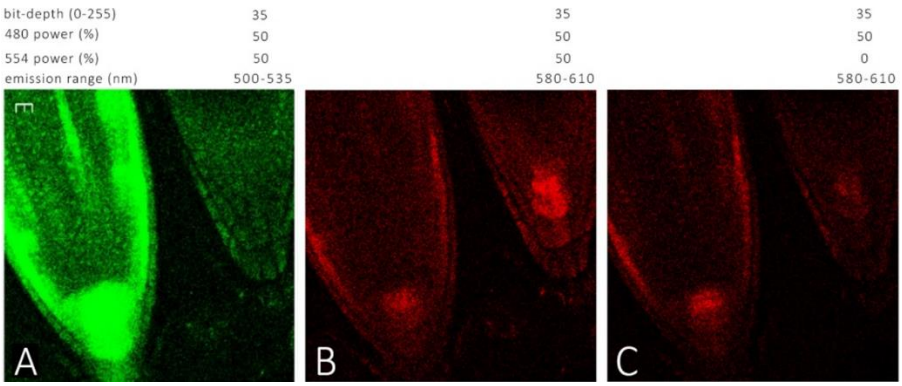

Figure 22: IAA33::GFP and IAA33::tdTomato in root tips. (A) Excitation of GFP at its emission range. (B) Excitation of tdTomato and redundant excitation of GFP at tdTomato's emission range. (C) Bleed-through test, GFP excitation at tdTomato's recommended emission range.

Thus GFP to tdTomato bleed-through does occur. For live-imaging twin embryogenesis this means that once GFP becomes active in suspensor-derived cells undergoing a transition to proembryo identity, GFP will excite tdTomato. This will be observed as an increase in tdTomato's fluorescent signal which may be interpreted as maintenance of suspensor identity whereas it actually is GFP to tdTomato bleed-through. However, this does not mean that double markers cannot be used for live-imaging suspensor-derived embryogenesis it rather means that when interpreting tdTomato's fluorescent signal, GFP to tdTomato bleed-through has to be taken into account.

To determine if GFP to tdTomato bleed-through decreases when tdTomato's emission range is shifted to longer wavelengths, eleven different emission ranges were set ranging from 560-590 nm to 660-690 nm (Figure 23A). For comparison, tdTomato is also excited over the same eleven emission ranges (Figure 23B).

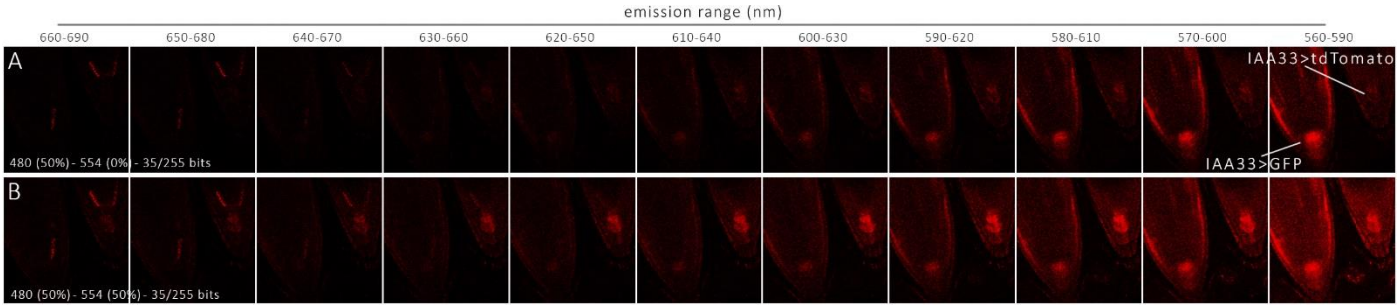

Figure 23: Recordings of tdTomato and GFP fluorescence in IAA33::GFP and IAA33::tdTomato *A. thaliana* root tips. (A) Sequence of 11 images where emission range is varied while roots tips are excited at 480nm with 50% laser power. (B) Sequence of 11 images where emission range is varied while root tips are excited with a WLL at 480nm and 544nm, both at 50% power.

GFP to tdTomato bleed-through is largest and roughly equal over four emission ranges. These emission ranges range from 590-620nm to 560-590nm (Figure 23A). When exciting both tdTomato and GFP, tdTomato's fluorescence intensity is largest at three emission ranges. These emission ranges range from 590-620nm to 570-600nm (Figure 23B). Therefore, the optimal emission range for capturing tdTomato's fluorescence when (live-)imaging GFP and tdTomato simultaneously is estimated to be between 570-620nm. However this emission range is roughly equal to range around tdTomato's emission maximum. Therefore, this result is largely redundant.

When plant screening for viable plants with double marker expression, only GFP's fluorescence was seen in the proembryo (Figure 24). In other words, pDRN was active and pCOBL6 was not active.

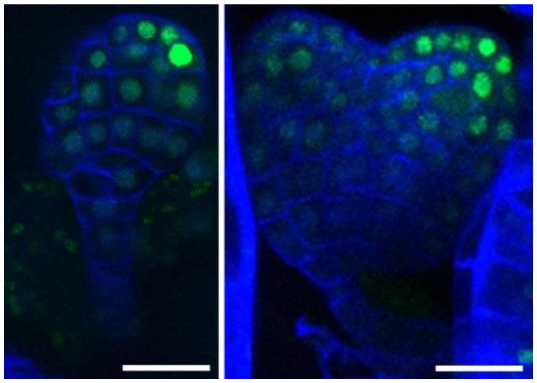

Figure 24: Popped embryos stained with Ren Dye of plants supposedly bearing a pDRN::GFP-pCOBL6::tdTomato construct. As can be seen only GFP signal is present. Scale bars are 20µm.

To test whether pCOBL6 was silenced, it was checked whether a part of the pCOBL6::tdTomato transgene (roughly 1100 bp) was present in thirteen different plants. This was done by extracting DNA from leaves using a CTAB extraction. A part of the pCOBL6::tdTomato transgene was amplified using polymerase chain reaction. The amplified DNA was run on gel.

On gel, a DNA fragment of roughly 1100 bp is seen clearly in lanes 2, 4 and 6, and not so clearly in 3, 5 and 7. In all other lanes 1, and 8 to 13, no fragment is seen (Figure 25). All plants have the same genome. Therefore, in theory, if the band is seen in one lane, it automatically means that all other plants have the construct too. However this is not seen on gel. It may be that the DNA concentration was too low to be visualized on gel. In any case, because the pCOBL6::tdTomato transgene fragment is most likely present it is assumed that pCOBL6 is silenced in the double marker line.

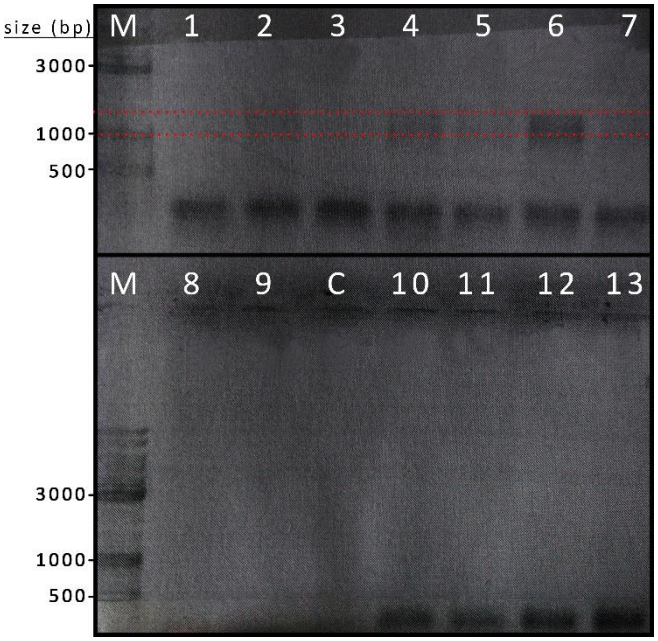

Figure 25: 2% agarose gel 0.5x TAE. M=marker. Numbers are the number of a pDRNpCOBL6 plant all with the same genome, C=Col-E DNA.

Discussion

live-imaging is time-consuming

To live-image twin phenotypes, both a strong fluorescent signal is required and twin phenotype has to be expressed. The former, strong fluorescent signal, is largely dependent on suspensor position. Generally, suspensors that are located close to the ovule's seed coat and close to the excitation laser have the strongest fluorescent signal. This is because the excitation laser and emission light will not have to penetrate through as many cell layers to reach the suspensors cells or detector, respectively. Unfortunately, the position of the suspensor is largely based on luck. When this luck factor is combined with a low twin phenotype penetrance, live-imaging as a tool to visualize twin phenotypes can become very time-consuming. To illustrate this, some data is shared. The data includes the amount of ovules screened for live-imaging and the amount of ovules that were selected from the ovules screened for live-imaging as well as the ovules with signal and from that the number of ovules with a good signal for the entire duration of the live-imaging experiment. Finally the number of ovules in which wrong division(s) were seen is shown too. Wrong division(s) only include wrong division(s) in suspensor cells other than the hypophysis because wrong division(s) in the hypophysis have never been shown to lead to twin seedlings.

Table 4: For two phenotypes, *twin1* and M0171>*bdl*, various data are given. The number of ovules that are screened as potential live-imaging candidates is shown. The number of ovules that show fluorescent signal at screening (ovules with signal) and the number of ovules with well-positioned suspensors are shown too (ovules with good signal). Percentages are percentages from the initial 'ovules screened' and are refered to in the text. *This number includes ovules in which M0171-GAL4 was crossed with UAS-*bdl* as well as ovules in which M0171-GAL4 was not crossed with UAS-*bdl*. Therefore, ovules with potential to show wrong divisions is not equal to ovules with good signal.

Phenotype	Ovules screened	Ovules live-imaged	Ovules with signal	Ovules with good signal	Ovules with wrong division(s)
Twin1	453	167	106	68 (15%)	7 (1.5%)
M0171>*bdl*	78	24	12	5 (15%)	2 (2.5%)

The percentage of ovules with good signal is 15%. Of these ovules with good signal 10% and 40% show wrong divisions for *twin1* and M0171>bdl, respectively. In turn, this is only 1.5% and 2.5% of the initial ovules screened, again, for *twin1* and M0171>*bdl*, respectively. This clearly illustrates the time-consuming nature of live-imaging suspensor-derived embryogenesis.

Another factor that determines whether wrong divisions can be observed during live-imaging is embryogenesis stage. In later embryogenesis stage, not only is the ovule's seed coat coloured green and thus inaccessible for the excitation laser, but suspensor activity may have progressed as far that suspensor identity is already lost or suspensors have died (Yeung, 1993). Therefore it is key that ovules are within stages of early embryogenesis, just before onset of wrong development. This is estimated to be around globular stage (Rademacher et al., 2012; Vernon & Meinke, 1994). To illustrate the developmental stage of ovules used here, a small sample was taken from the ovules screened for live-imaging and it was determined that embryo stages ranged from 4-cell stage to mid-globular stage (Figure 26).

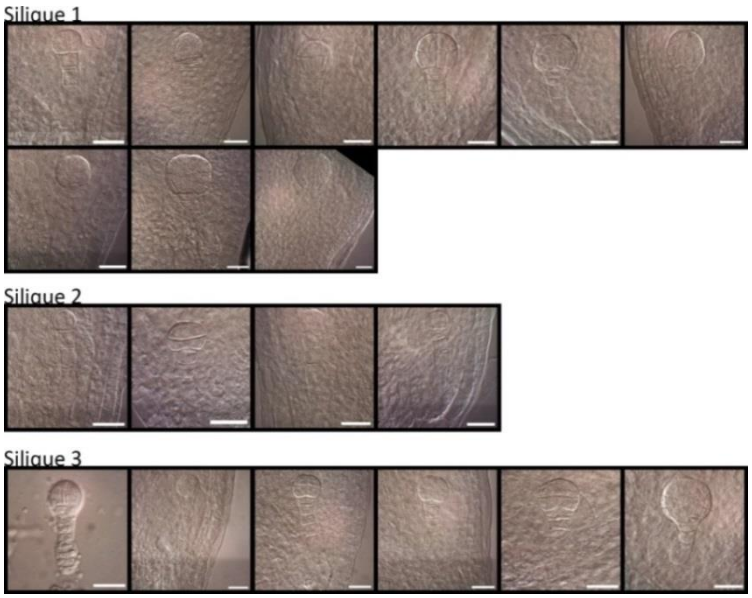

Figure 26: DIC images of embryo stage at the start of *in-vitro* culturing and live-imaging for three different siliques. Scale bars are 20 µm long.

Interpretation of live-imaging results

Ideally for correct interpretation of time-lapses, the suspensor is completely aligned with the confocal plane. However, most of the time this is not the case and the suspensor is located at a slight angle (Figure 27). Interestingly, when not all suspensor cells aligned it the most basal, and largest, suspensor cell that is missing (Figure 28). Thus it may be clear that signal intensities within suspensor cell nuclei vary between z-slices (Figure 28). This illustrates that only a slice of the entire fluorescent signal emitting from the suspensor-cell nuclei is seen in each z-slice. Although 10µm distance between z-slices is optimal in most cases, sometimes a larger z-resolution is required to accurately assess whether fluorescent signal intensity changes. To correctly interpret changes in fluorescence a 3D image of the suspensor cell nuclei would have to be made. From there signal intensities can be quantified before determining whether fluorescent signal intensity changes. However, high-resolution 3D imaging of suspensor cell nuclei is time-consuming and therefore impractical for live-imaging twin phenotypes because only one hour is available before a next recording has to be made. To add to this, this has to be done for twenty to thirty ovules because a large number of potential ovules to express twin phenotype have to be live-imaged because twin phenotype penetrance is low. To further complicate the matter, suspensor cell nuclei are prone to movement. Mostly, suspensor cell nuclei move in a zig-zag like motion (not shown, may be visible in Movie S1 and S2). Additionally, division planes in aberrant phenotypes may make complex cellular structures. Both the suspensor cell nuclei movement and the complex cellular structures may additionally complicate interpretation of fluorescent signal intensities.

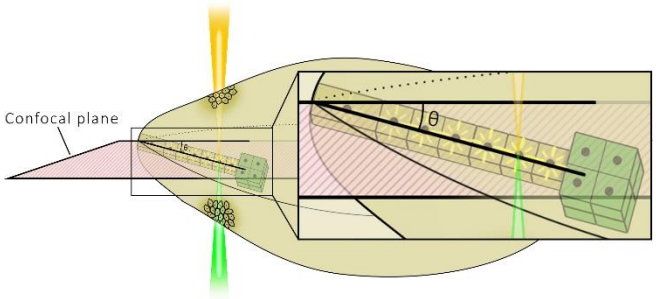

Figure 27: Illustration of suspensor being at an angle relative to the confocal plane.

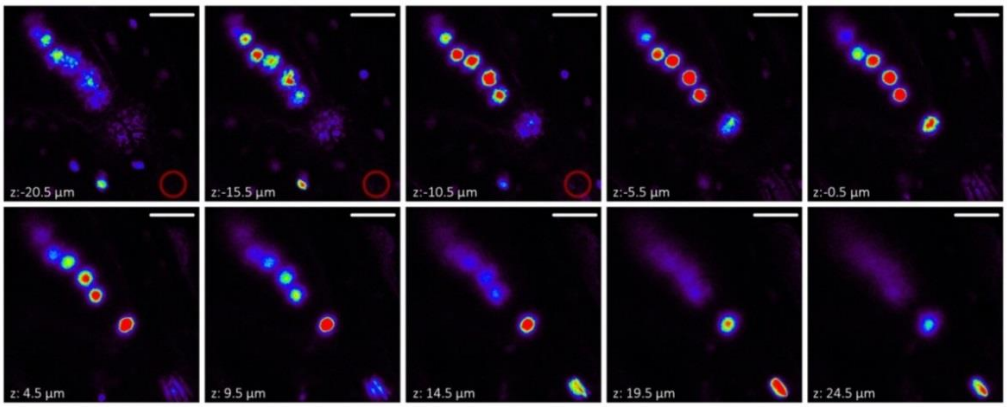

Figure 28: Fluorescent signal emitted from suspensor cells scattered over multiple z-planes. The most basal located suspensor cell is marked in a red circle when invisible. Scale bars are 20µm.

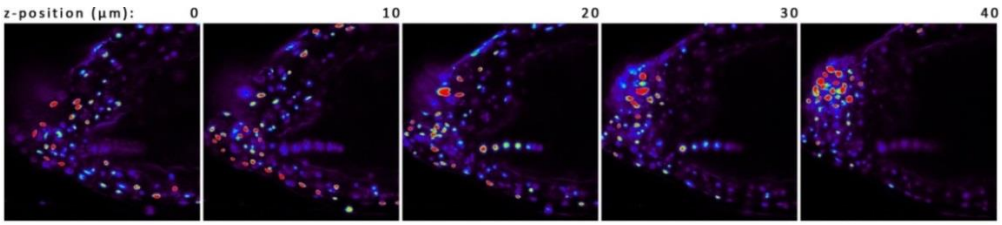

Figure 29: Fluorescent signal emitting from suspensor cells scattered over multiple z-planes.

Next to differences in fluorescent signal intensity, the markers and model phenotypes used differ too. Both promoters of the markers, WRKY2 and ATPase, are linked to suspensor cell identity. Although the degree as to which each gene is linked to suspensor identity remains elusive because only WRKY2 has been proven to be linked to suspensor identity whereas for ATPase this is merely an assumption because its expression pattern is restricted to the suspensor. In any case, there may be different routes *twin1* and M0171>*bdl* take to acquire proembryo identity starting from suspensor identity. In turn, this may mean that, for example, WRKY2 activity can be shut-off at a different time-point in *twin1* than in M0171>*bdl* but also that ATPase can be shut-off at a different time-point in

M0171>*bdl* compared to WRKY2 in M0171>*bdl*. The former can be elucidated by observing WRKY2 activity in *twin1*. However, in the latter case, a comparison is made between two distinct genes that are both regulated by their own set of regulators in an aberrant environment. Therefore, when theoretically expressing WRKY2 and ATPase in the same model phenotype, the time-points at which ATPase and WRKY2 shut-off may differ but is a result of difference in gene regulation.

Twin1 and M0171>bdl penetrance literature comparison

From (Table 4) *Twin1* and M0171>*bdl* penetrance is determined to be 12% and 40%, respectively. Twin phenotype penetrance is determined by putting ovules with wrong division(s) over ovules with potential to show vertical division(s).

Previously, *twin1* penetrance of 9% was observed by growing *twin1* seeds on MS plates (Vernon & Meinke, 1994). Subsequently, the number of twins was observed after seed germination. The difference between 12% and 9% is minimal. However, whether all ovules in which wrong division(s) occur eventually give rise to polyembryonic plants is questionable. Therefore, it is difficult to say whether the two twin phenotypes penetrance percentages resemble the same phenomenon.

M0171>*bdl* has a penetrance of 40%. Previously, M0171>*bdl* has been shown to have aberrant development in 31% of embryos in early embryogenesis up to 81% at heart stage (Rademacher et al., 2012). Live-imaging of M0171>*bdl* was started 74 hour after pollination. Therefore, at the start of live-imaging embryos are expected to be around early globular stage. Live-imaging was continued for 62 hours. After 62 hours it is expected that heart stage is reached and thus that M0171>*bdl* penetrance should be higher. The large difference in M0171>*bdl* may be attributed to self-pollination. All plants pollinated with pollen from a plant line containing a UAS-*bdl* line were marked, however, self-pollination could still have occurred beforehand. It is expected that if more live-imaging experiment are carried out the M0171>*bdl* phenotype penetrance may rise.

Difference in ovule viability in literature

Here, an OSR of 0.42 is measured in non-channeled PMDs after live-imaging for 62-69h and an OSR of 0.71 in channeled PMDs after live-imaging for 67-69h. Previously, an ovule survival rate of 0.4 was measured for *in-vitro* cultured ovules after 72h (Figure 30, purple bar) (Gooh et al., 2015). These ovules were cultured in the same *in-vitro* culturing medium. However, the method of culturing and assessment of ovule viability differed. Ovules were submerged in live-medium in a round dish and cultured in a growth chamber. Ovule viability was assessed by detection of marker fluorescence in embryos or autofluorescence of the integuments.

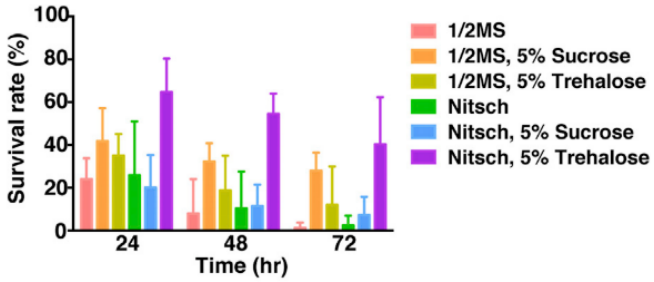

Figure 30: Ovule survival rate in different culturing media. Nitsch supplemented with 5% trehalose is the same as live-medium. Data was taken from an article written by (Gooh et al., 2016).

Because in the assessment of (Gooh et al., 2015) ovules were submerged, the effect of live-medium on ovules is most similar in ovules in channelled PMDs. Given that survival rate and OSR represent the same, the previously measured survival rate is lower compared to the survival rate measured here (0.4 versus 0.71). The large difference may be attributed to the method of determining ovule viability. It is expected that assessing ovule viability by detection of (auto)fluorescence is more accurate. In turn, this may result in lower ovule viability rates. Additionally, growth conditions may have also affected ovule viability. Here ovules were cultured while live-imaged and the temperature in the confocal microscopy room is expected to be lower than in a growth room (exact temperatures unknown). Growth room temperature is expected to increase ovule viability because it better resembles the natural conditions *A. thaliana* ovules reside in. Surprisingly, it does the opposite, ovules in the colder than natural conditions live longer. Because this is inexplicable, more insight into preparation of ovules in a dish and the calculation to determine survival rate is required. Thus, comparison between OSR and survival rate is interesting, but, for now, the two are not comparable.

Ovule growth comparison with literature

The ovule growth in PMDs was compared to ovule growth in flexible PDMS cages (Figure 31) (Park et al., 2014). Ovules placed in the cages were collected at developmental stage 16 according to (Smyth, 1990), whereas ovules in PMDs, were, like described in 'live-imaging is time-consuming', around 4-cell stage to mid-globular stage. Which exact embryogenesis stage developmental stage 16 according to (Smyth, 1990) is, is unknown.

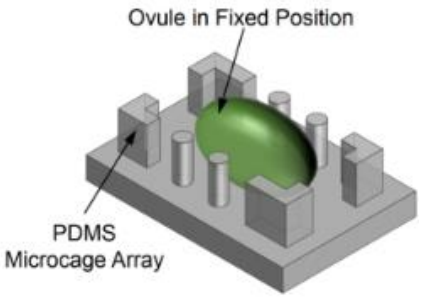

Figure 31: Ovule inside a PDMS ovule cage. Image taken from (Park et al., 2014).

In cages ovules were measured 341µm in major axis and 174.8µm in minor axis at the start of *in-vitro* culturing. After 5 days, ovules grew up to 526.7 µm in major axis and 338.8µm in minor axis in 650µm long, and 200µm wide cages. In 650µm long, and 250µm cages ovules grew up to 546.3µm and 317.4µm in major and minor axis respectively. Whereas in PMDs, on average, at the start of live-imaging, ovules are 382µm and 245µm long in the major axis and minor axis, respectively. And during 45-84 hours of live-imaging, ovules, on average, grow up to 430µm and 289µm in major axis and minor axis, respectively.

There is a significant difference in starting length of minor axis between ovules cultured in cages and ovules cultured in PMDs. This may be explained by ovules in PMDs being introduced at a later developmental stage than ovules in cages.

It was checked if ovule growth in cages can be linearly aligned with ovule growth in PMDs. This was not the case (Figure 32). There is less major axis growth in PMDs compared to cages. This may be explained by the fact that cages were 650µm long and 200µm or 250µm wide. Therefore, ovules in cages had more potential to grow in their major axis compared to ovules in PMDs, where the distance between micropillars is 300µm or 350µm. Contrarily, minor axis growth is slower in PMDs but minor axis was at all times larger in PMDs. This, again, can be explained by the physical restrictions imposed by the culturing device, only in this case the cages impose a physical restriction because with a width of 200µm or 250µm and not the PMDs.

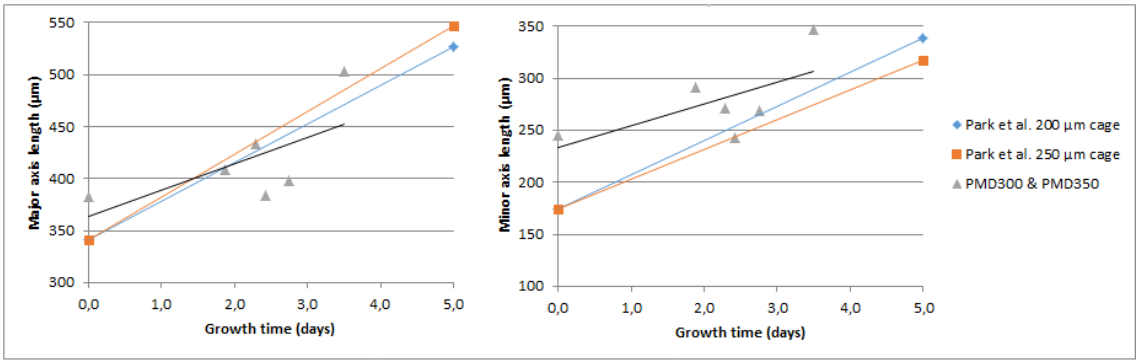

Figure 32: Major and minor axis growth over 5 days for Park *et al.*'s data and data obtained here. For Park *et al.*'s data only two time points were available: t=0 and t=5 days. For data obtained here, growth data at time points of t=0, 1.9, 2.3, 2.4, 2.8, and 3.5 days were available.

It may be clear that culturing devices can affect or stunt ovule growth. This may additionally be confirmed by observations of ovules growing to be round rather than oval (Movie S3). Although this was not seen regularly, it was most seen when ovules were growing close to the walls of the PMD.

Oddly enough, imposing growth restrictions on ovules could alter their growth direction which ultimately may be used to alter suspensor position to enhance accessibility of fluorescent proteins and in turn increase the percentage of ovules with good signal. However, this is of course purely speculative because imposing growth restrictions may affect ovule survivability more negatively by providing a rather uncomfortable growth environment than actually enhance live-imaging.

Conclusion

Lastly, it can be concluded that live-imaging is a viable method for observing changes in cell identity during (twin) embryogenesis, but it is also a method that requires care of delicate ovules and may be (very) time-consuming. Luckily, taking care of delicate ovules has been partially optimized by altering the PMD design which enhanced live-medium flow and subsequently ovule survival rate. Next, the reward from live-imaging is great when a well position suspensor is captured that has, in addition to a great suspensor cell nucleus signal, also twin phenotype penetrance, which makes the time-consuming factor redundant.

From the captured time-lapses can be concluded that in M0171>*bdl* suspensor identity appears to be maintained post wrong division and in *twin1* suspensor identity is lost post wrong division. Loss of suspensor identity is expected to be a gradual process. Therefore, these observations may be linked to the fact that WRKY2 and ATPase carry out different functions within the cell and that ATPase activity is lost earlier in this gradual process. However, both markers were also imaged in different phenotypes which may additionally contribute to the fact that there are differences in maintenance of suspensor identity.

Next in the mission to elucidate when proembryo identity is acquired, a double marker should be used. Unfortunately, the double marker used here showed silencing of the proembryo-specific component. However, with an eye on the future, at least, now it has been confirmed that using GFP and tdTomato double markers can cause fluorescence bleed-through from GFP to tdTomato. In turn, this may affect the interpretation of live-imaging results, but knowing that GFP to tdTomato bleed-through occurs, this can be taken into account when viewing live-imaging results.

Recommendations

A new double marker line may be generated to determine when in addition to providing more evidence to when suspensor cell identity is lost also help in determining when proembryo identity is acquired. The double marker used here was generated from a single transgene. It was proposed by Tatyana Radoeva that introducing two marker constructs individually may prevent silencing.

To identify if WRKY2 activity shuts down later in aberrant development, time lapses have to be made in which more rounds of cell divisions are visualized. Additionally, both markers may be introduced in both *twin1* and M0171>*bdl* to identify if WRKY2 or ATPase activity is lost at different time-points.

To ultimately determine the exact moment of suspensor cell identity loss, quantification of fluorescent signal intensity is a must. Once quantified, the decrease in fluorescent signal intensity can be linked to fluorescent protein half-life and ultimately give a good estimation of when fluorescent protein production was stopped.

Because the division planes in aberrant phenotypes can be odd when compared to wild type it may be useful to add a membrane marker to distinguish wrongly divided cells. Additionally, when a membrane marker is added that is linked to a promoter that is neither specific for suspensor or proembryo identity, the membrane marker will show cells with no marker activity. This is most useful in lines with only a suspensor marker to determine what happens to cells after suspensor identity loss. In double marker lines a membrane marker may lose this function.

Acknowledgements

Firstly I would like to thank Tatyana Radoeva for her help with seed sterilization, seed plating, twin selection, confocal microscopy, DNA extraction and gel electrophoresis as well as answering questions and providing feedback on the report several times. Next I would like to thank Thijs de Zeeuw for his help with starting live-imaging and providing PMDs. Jan Willem Borst and Adrie Westpal I would like to thank for sharing their expertise in confocal microscopy. Lastly I would like to thank Sacco de Vries for his help with showing how to prepare for live-imaging and preparing live-medium solutions as well as answering questions and providing feedback on the report.

Supplemental information

Supplemental figures

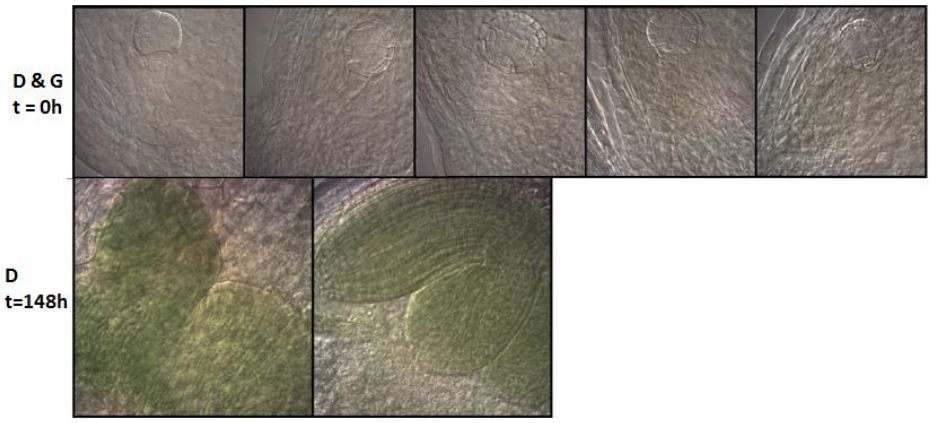

Figure S1: Embryogenesis stage of ovules from (Figure 11D and G) at the start of *in-vitro* culturing and after 148 hours.

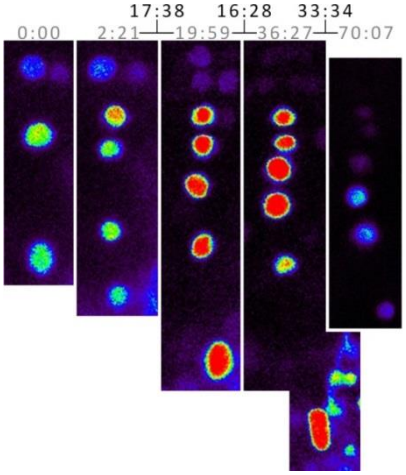

Figure 19: Estimation of suspensor cell cycle. Four consecutive suspensor cell divisions (wt). The last cell division, that is barely visible, took 33 hours. This seems more like the amount of time in which two cell divisions occur. It could be that one cell division was not captured during the time-lapse. However, in that case the amount of cells would still have to increase and this is not the case. Therefore, it could also be that cells were located on top of each other and therefore not visible.

Supplemental movies

For the creation of the supplemental movies, LAS X was used to select z-slices with highest intensity of fluorescent signal emitting from suspensor cells per time-point. In some cases multiple z-slices were selected because highest intensity of fluorescence per suspensor cell was scattered over multiple z-slices. In this case, a maximum projection was generated over these selected z-slices. z-slices or maximum projections were then aligned chronologically. The generated project was exported as a 7 frames/second .avi file with time code and scale bar options enabled. Below, in (Table S1) are the experted .avi file names used per supplemental movie in the order in which they appear in each supplemental movie. The numbers in the filename represent: <day of live-imaging experiment>.<month of live-imaging experiment>.<position of the ovule in LAS X's mark&find module>. Unaltered files can be viewed in the twin1-phenotypes.lif file. Experted .avi files were edited in Adobe After Effects CC 2015.

Table S1: .avi filenames of ovules used in each supplemental movie in the order in which they appear in each supplemental movie. The first number corresponds to the day of live-imaging, the second number corresponds to the month in which the live-imaging experiment took place and the last number is the position of the ovule in LAS X's mark & find module. Ovules have been named similar in the twin1-phenotype.lif file.

Movie	Ovule 1	Ovule 2	Ovule 3	Ovule 4	Ovule 5	Ovule 6
S1	9.5.6	6.7.17	9.5.2 & 11.5.2	9.5.4 & 11.5.4	9.5.13 & 11.5.13	6.5.7
S2	28.9.2	28.9.7				
S3	12.04.12	12.04.8	12.04.7			

Description of supplemental movies:

Movie S1: pATPase>Venus in *twin1*. Six ovules with wrong suspensor cell divisions.

Movie S2: pWRKY2>Venus in M0171>*bdl*. Two ovules with wrong suspensor cell divisions.

Movie S3: Odd ovule growth.

Supplemental protocols

Supplemental protocols includes protocols on starting up the microscope and configuring LAS AF and LAS X for image acquisition or live-imaging. These protocols were originally written for the materials & methods section. Therefore, some of the figures and some of the text is the same as in the materials & methods section. However, after revision, the materials & methods was updated to its current state. These protocols serve as a more detailed, instructive, version of methods.

Starting up sP5 confocal microscope

Following order given in Figure A1; turn on PC microscope and wait until movement of microscope's stage stops, turn on scanner power, laser power, and switch laser emission key from off-0 to on-1.

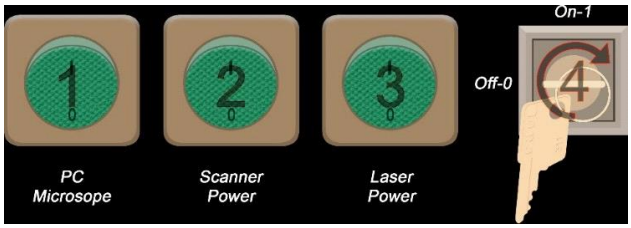

Figure A1: Button panel of sP5 and sP8 Leica's confocal microscope. To power the Leica's microscope(s) turn on hardware following numeric order given.

Log in on PC as *TCS user* with password *'tcsuser'*. Start *LAS AF* software. A pop-up window will appear, click 'OK'. Another pop-up window will appear asking to calibrate microscope's stage. Ensure that microscope's stage is clear from objects. Click 'YES'. Go to *LAS AF>configuration tab>Lasers*. Check *'argon'* checkbox and put its *'power output'* to 20%.

LAS AF image acquisition

In LAS AF, configure acquisition settings; go to Acquire>Acquisition. Click 'seq.' button (Figure A3A). Add a second scan; click '+' button (Figure A3B). Select scan 1. Configure scan 1's 'Beam Path Settings' for Ren Dye. Increase 405 power to 5% (Figure A3C); Select RT30/70 mirror, activate HyD 1, and set HyD 1's emission range to 430-460 nm (Figure A3D). Select scan 2. Configure scan 2's 'Beam Path Settings' for Venus; increase 514 laser power to 20% (Figure A3C); Select DD 458/514 mirror, activate HyD 3, and set HyD 3's emission range to 550-600 nm (Figure A3E). Different FPs require different 'Beam Path Settings'; (Table A1) shows settings required for GFP and tdTomato.

Table A1: LAS AF acquisition settings for Ren Dye, GFP, Venus and tdTomato.

Fluorescent protein	**Laser type**	**Excitation λ (nm)**	**Emission λ (nm)**	**Mirror**
Ren dye	Diode	405	430-460	RT30/70
GFP	Argon	488	500-535	RSP500
Venus	Argon	514	550-600	DD458/514
tdTomato	Argon	554	560-590	DD488/561

Change acquisition settings in 'XY' panel to mimic settings shown in Figure A3F. Select scan 1. View popped embryo on-screen; click on 'Live' (Figure A3G). Put embryo in confocal plan by adjusting z-position with Leica's 6 knob panel (Figure A2). Start imaging; click 'Start' (Figure A3G). Two screens images appear; top is scan 1, bottom is scan 2.

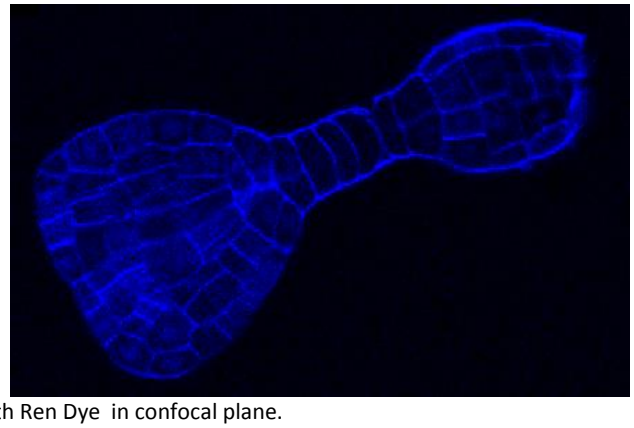

Figure A2: Popped embryo, stained with Ren Dye in confocal plane.

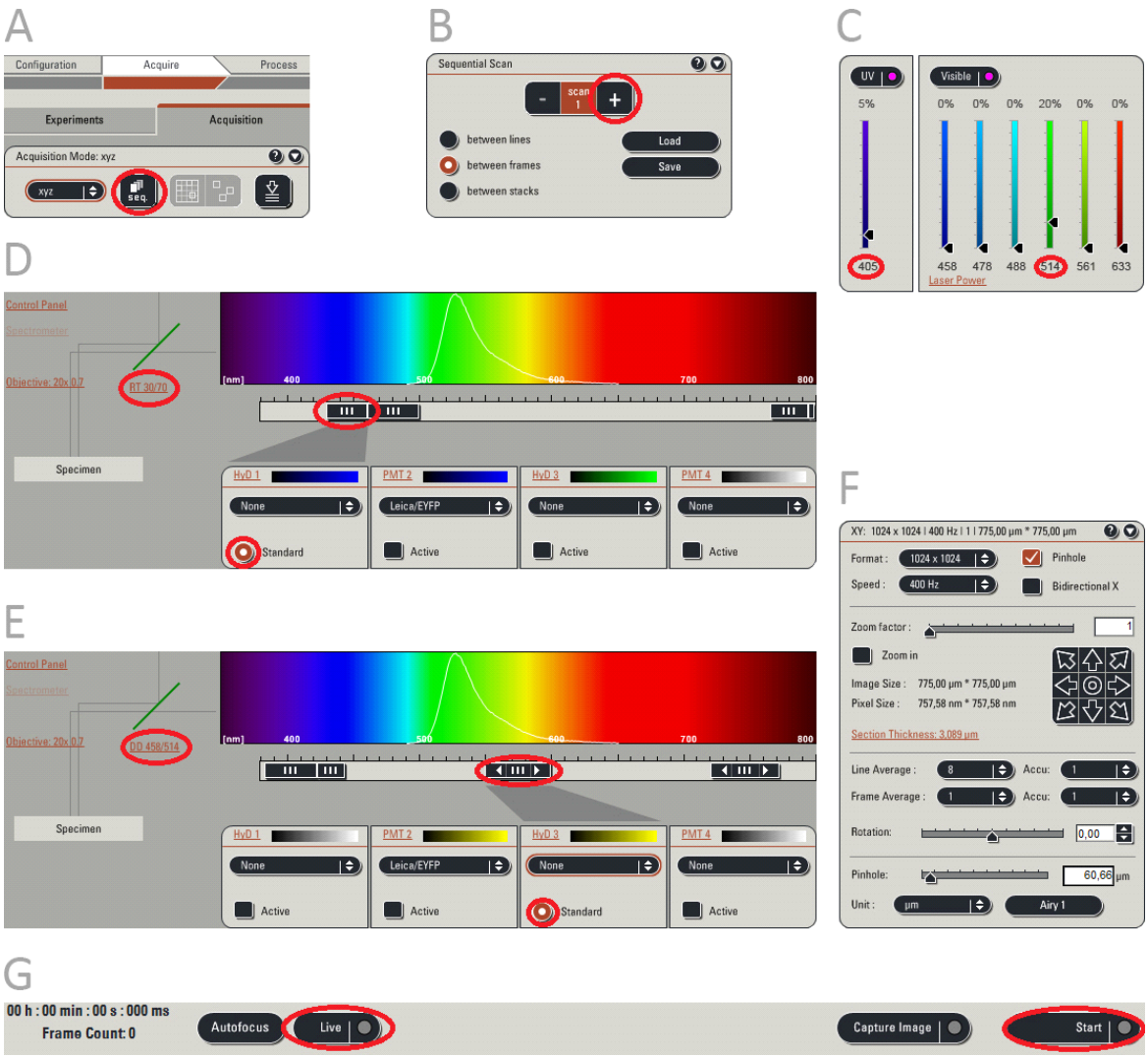

Figure A3: Parts of LAS AF's user interface. (A) Acquisition panel. (B) Sequential scan panel. (C) Beam Path Settings's Laser power control panel. (D and E) Beam Path Setting's mirror, HyD or PMT, and emission range control. (F) Image acquisition panel. (G) Bottom panel.

Cleaning and sterilization

Remove 'Live'-medium from the imaging chamber. Flip the micropillar device(s) up-side-up and remove and 'Live'-medium from micropillar device(s). Remove all ovules from the micropillar device(s) using a 0.6 x 25mm (blue tip) dissecting needle. Transfer micropillar device(s) to a round-bottom dish. Remove left-over ovules from imaging chamber. Put the round bottom dish containing micrpillar device(s), imaging chambers and both lid of imaging chamber and round bottom dish in a 120mm square petri dish. Fill square petri dish, imaging chamber, round bottom dish, and both lids with 75% ethanol. Leave petri dish for 30min. Remove ethanol from all equipment and leave it to dry for 30min. Irradiate all equipment with UV-light for 30min. Flip micropillar devices, and, again, irradiate all equipment for 30min with UV-light. Put lid of petri dish on petri dish, seal it with tape to label it sterile.

Live-imaging

Start Leica's sP8's confocal microscope. Leica's sP8 hardware is similar to Leica's sP5 hardware. Thus, start up Leica's sP8 confocal microscope following instructions from (Starting up sP5 confocal microscope, pg.27). Differences between starting up sP5 and sP8 are software used, LAS X replaces LAS AF, and a white light laser(WLL) replaces diode and argon laser. Turn on WLL by turning the key on WLL box from off to on. When starting up LAS X, two pop-up windows will appear (Figure A4). The first pop-up window is for hardware configuration settings, just click 'OK'. The second pop-up window asks to calibrate the microscope's stage. Click 'YES' because stage calibration is necessary for LAS X's 'Mark and Find' function, explained at Manual ovule screen, pg.29, to function properly.

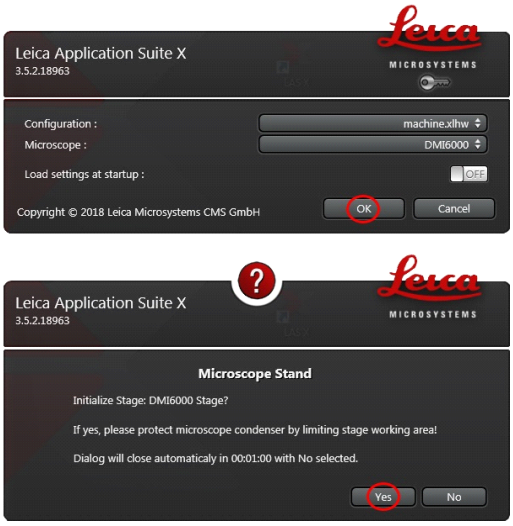

Figure A4: Two LAS X's start-up pop-up windows. Upper one is first pop-up window. Lower one is second pop-up window.

Select 20x objective with "CHG OBJ" button on right side of micropscope's stand. Immerse entire objective's surface with 20% glycerol. Covering entire surface is necessary because glycerol evaporates during measurements exceeding 12h. Lock imaging chamber on microscope's z-galvo stage. Lower z-galvo stage with salt & pepper shaker joystick until imaging device touches glycerol immersion.

In LAS X, go to Configuration>Laser Config. Turn WLL on and, if not already set to 50%, set power to 50% (Figure A5A). Go to Acquire>Open Projects>Open Project. Open a project with 'preset' files containing acquisition settings to be used. Right click on a preset file and click 'apply image settings' (Figure A5B). If no preset files are available go to Acquire and configure new acquisition settings (Figure A5C).

Here a description for configuring acquisition settings for Venus is given. In Table 3 acquisition settings for GFP and tdTomato are also given. Turn on or create a 514 nm WLL excitation beam. Put 514nm WLL excitation beam's power to 25%. Turn on one of three HyDs and drag the start of their emission band to 535nm and extend it to 570nm. Select a Lookup Table(LUT) (e.g. Spectrum) by double-clicking on the small circle (Figure A5C). Leave gating off, set gain to 150%, and turn BrightR on (Figure A5C). Gating only lets through emission light after the set amount of time has passed. Gain can be used to increase signal intensity. BrightR makes bright, dimmer and dim, brighter.

Figure 5A: Various parts of LAS X's user interface. (A) 'Laser Config'. (B) 'Open Projects'. (C) 'Acquire'. (D) Bit-depth slide bar.

Manual ovule screen

Switch to bright field(BF) using *TL/IL* button on left side of microscope's stand. Look through ocular and put sample in-focus by adjusting z-position. Search for ovules. Center found ovule and view it on-screen in LAS X by clicking 'Live'. Place fluorescent signal emitted from marker in confocal plane by lowering or lifting z-position (Figure 9). Difficulties may arise when searching for marker. Three factors that can determine marker presence are, embryo location within ovule, homo or heterozygosity of inserted construct and frequency of phenotype. The latter two are screened for beforehand according to Plant screening, pg.3. However, when an embryo is located towards the top of an ovule, signal emitted from marker has difficulty penetrating cell layers below and reaching the detector (Figure 5).

Additionally, signal intensity may not be optimized. To adjust amount of excited FPs, adjust WLL's excitation beam's power. Alternatively, to artificially increase signal intensity on-screen, decrease bit-depth (Figure 7D). Lowering bit-depth decreases amount of shades displayed, shades of green become green, whereas shades of black become black. Additionally, to decrease noise and autofluorescence signal, raise bit-depth's lower threshold (Figure A5D).

Continuing with an ovule with a marker, increase 'Zoom Factor' 2.5 - 3.0x (a zoom beyond 3.5x will artificially increase the level of detail) and centre marker signal. Go to Acquire>Acquisition>Acquisition Mode, select xyzt from the dropdown menu and click 'Define Mark and Find Experiment' button (Figure A6A).

Go to Acquire>Acquisition>Stage, click 'Mark positions' and uncheck 'Same stack for all' checkbox. A new button, 'Redefine Stack', appears in the stage window (Figure A6B). Go to Acquire>Acquisition>Z-Stack (Figure A6C). Place confocal plane at top end of marker signal, round 'Z-position' to its closest tenth, and click 'Begin'. Place confocal plane at bottom end of suspensor, again, round 'Z-position' to its closest tenth, and click 'End'. Click 'Z-Step Size' option and set to 10.00 µm. To assign the just-created custom Z-stack for position 1 to position 1, go back to Acquire>Acquisition>Stage and click 'Redefine Stack' (Figure A6C). Repeat from 'Manual ovule screen' for every ovule in PMD (screening 20 ovules takes ~30min). Finally, when all ovules to be imaged are marked, you have the possibility to save their locations (Acquire>Acquisition>Stage>Save). Saving is useful when re-using the same sample at another time; for example: when checking for fluorescent signal the next day.

Automated ovule screen

Because screening through ovules is laborious, an automated ovule screen will save time and keep you focused. Thus, alternatively to 'Manual ovule screen', an automated ovule screen can be performed using a z-stack tilescan of PDM's inner area (Figure 8).

To perform a z-stack tilescan, go to Acquire>Acquisition>Acquisition Mode and select xyz from dropdown menu and activate 'Define Tilescan Experiment' (Figure A7A).

To create the tilescan: turn on BF, look through ocular and position top-left of inner area in the middle. Go to Acquire>Acquisition>Stage and click 'Mark Positions' (Figure A7B). Look through ocular and position bottom-right of inner area in the middle and again, click 'Mark positions'.

To create the z-stack: similar to 'Manual ovule screen', select an ovule, place the confocal plane at, this time at top-end of ovule instead of top-end of marker signal and click 'begin' (Figure A6C). Place confocal plane at bottom-end of ovule and click 'end'. Try to minimize the amount of steps because it increases imaging time significantly. For example, a 11 slice z-stack of a 9x9 tilescan takes ~30min. 'Z-step size' should be around 30µm to ensure all potential ovules are screened.

Go to Acquire>Acquisition>XY. Configure acquisition settings to mimic Figure A7C. Acquisition settings in Figure A7C are optimized to detect marker signal while keeping image quality low. This is done to lower imaging time. Additionally, 'Bidirectional X' can be turned on to further decrease screening time. 'Bidirectional X' instructs the laser to scan from left to right, and from right to left, whereas, when 'Bidirectional X' is turned off, the laser scans from left to right, returns to the left and, again, scans from left to right.

To find ovules with marker signal, look at the completed z-stack tilescan, mark ovules with marker signal (Figure 8). Locate marked ovules in PMD by looking through the ocular while keeping in mind that images taken are rotated 90° clockwise and continue from 'Manual ovule screen' only for marked positions.

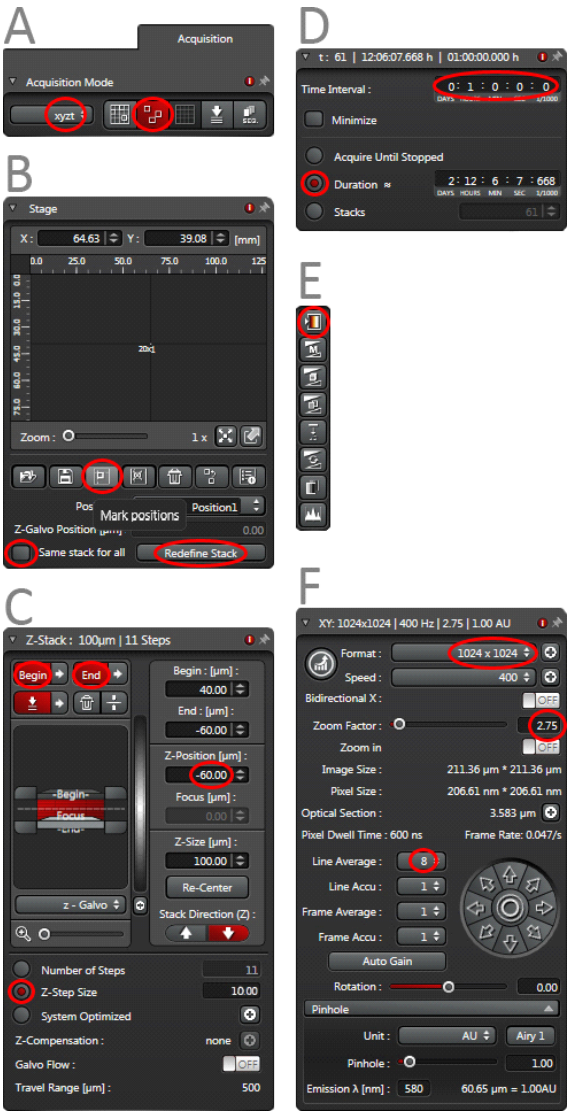

Figure A6: Various parts of LAS X's user interface used during manual ovule screen. (A) Acquisition mode. (B) Stage window. (C) Z-Stack window. (D) t-window. (E) Over-/Underexposure button. (F) XY-Window, for customizing image acquisition settings.

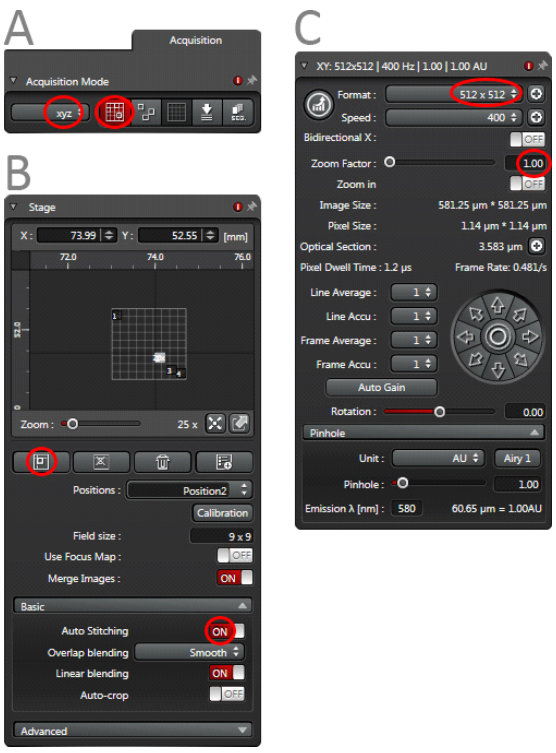

Figure A7: Parts of LAS X's user interface used during 'Automated ovule screen'. (A) Acquisition Mode. (B) Stage-window. (C)XY-window, for customizing image acquisition settings.

Image processing with Fiji (ImageJ)
Programs required: Fiji (ImageJ version 1.51p), Java (version 1.8.0_66 (64bit))

Start up your *<filename>*.lit file with Fiji. A *Bio-Formats Import Options* window will pop up, here, click *ok*. In the following *Bio-Formats Series Options* window, select images or time-lapses to work with and click *ok* (loading multiple time-lapses at once may take some time).

Multiple edits can be made to the time-lapses, all of them are optional; below a couple are mentioned. Try to follow the order in which they are given to avoid conflicting actions, e.g. adding a time-stamp, then cropping, resulting in cropping out the time-stamp. It should be noted that for movies made in results, LAS X image processing was used and not ImageJ's. However, ImageJ provides similar features as LAS X and a lot more.

Lookup Table(LUT)
To distinguish regions with intense marker signal from regions with weak regions of FP signal with more colours, a lookup Table(LUT) can be placed on top of a grayscale image. To do this, *Image>Lookup Tables><Select your lookup Table of choice>*. I prefer '3-3-2 RGB' or 'Fire'. Here, as an example, 3-3-2 RGB is used (Figure A8A).

Rotation
To rotate an image; *Image>Transform>Rotate*. Hit Preview to see how many rotation changes the image. For convenience, it may be nice to rotate all time-lapses with micro pillar ends facing bottom (Figure A8B).

Merging maximum intensities of z-slices into a z-project
Because suspensor cells are not always aligned in the same z-slice, maximum intensities of z-slices can be merged into one z-project; to do so: *Image>Stacks>Z Project*.

Each z-slice to-be-put into the z-project contains fluorescent signals from different cells of a suspensor. For example, in (Figure A8C), upper suspensor cells are better aligned in slice 10/17, while lower suspensor cells are better aligned in slice 12/17.
In ZProjection window (Figure A8C), at *start slice*: enter the first slice you want to include in your z-project. At *stop slice*, enter the last slice to include. Select 'Max intensity' from 'Projection type' dropdown menu. Leave *'All frames'* checkbox checked. Click *'OK'*. A new window will open with the generated z-project.

Cropping
To crop the image; select the 'rectangle tool' (Figure A8D) and use it to mark the region to be cropped. Now press 'ctrl+shift+x'. Cropping images decreases file size, which, when working with large amounts of time-lapses, can significantly decrease storage space. However, when cropping, do keep in mind, that sometimes, later in time-lapses ovules can move slightly; so don't crop out too much.

Time-stamp
To add a time-stamp; *Image>Stacks>Label*. In (Figure A8E), 'Format' can be 00:00:00. The starting value is the time at which the first image was taken, enter time in seconds. The 'Interval' is the time between each consecutive t-slice, this is the same as the 'time interval' entered in LAS X, again, here, enter time in seconds. 'X- and Y-location' is where the time-stamp will be created on the image; in the box you can change the location; X5-Y20 is the top left.

In 'Text' box enter anything to label the image. Text will appear after the time-stamp. In 'Range' enter the range of images the time-stamp should appear on.

By checking 'Use overlay', the label is be placed in a separate layer, the overlay, on top of the time-lapse images layer instead of, when not checking 'Use Overlay,' engraved onto the image. Checking 'Use Overlay' is useful to later edit the label. To edit the label, first remove the overlay, *Image>Overlay>Remove Overlay* and generate a new label, *Image>Stacks>Label*.

Scale bar
To add a scale bar; *Analyse>Tools>Scale Bar*. In the *Scale Bar* window customize the to be created scale bar (Figure A8F). The Scale bar customization options given speak for themselves. Here, again ensure to check the 'Overlay' box. And check the 'Label all slices' checkbox.
Saving

To save the edited time-lapse; *File>Save As>Tiff*. .tiff format saves t-slices, z-slices, and overlay in separate layers in contrast to. jpeg images which saves one slice, or .gif which saves both t- and z-slices in one layer. .tiff format also compresses data in the most efficient way when compared to the other options available by imageJ: .avi and .raw, to keep file size, relative to these two formats, low.

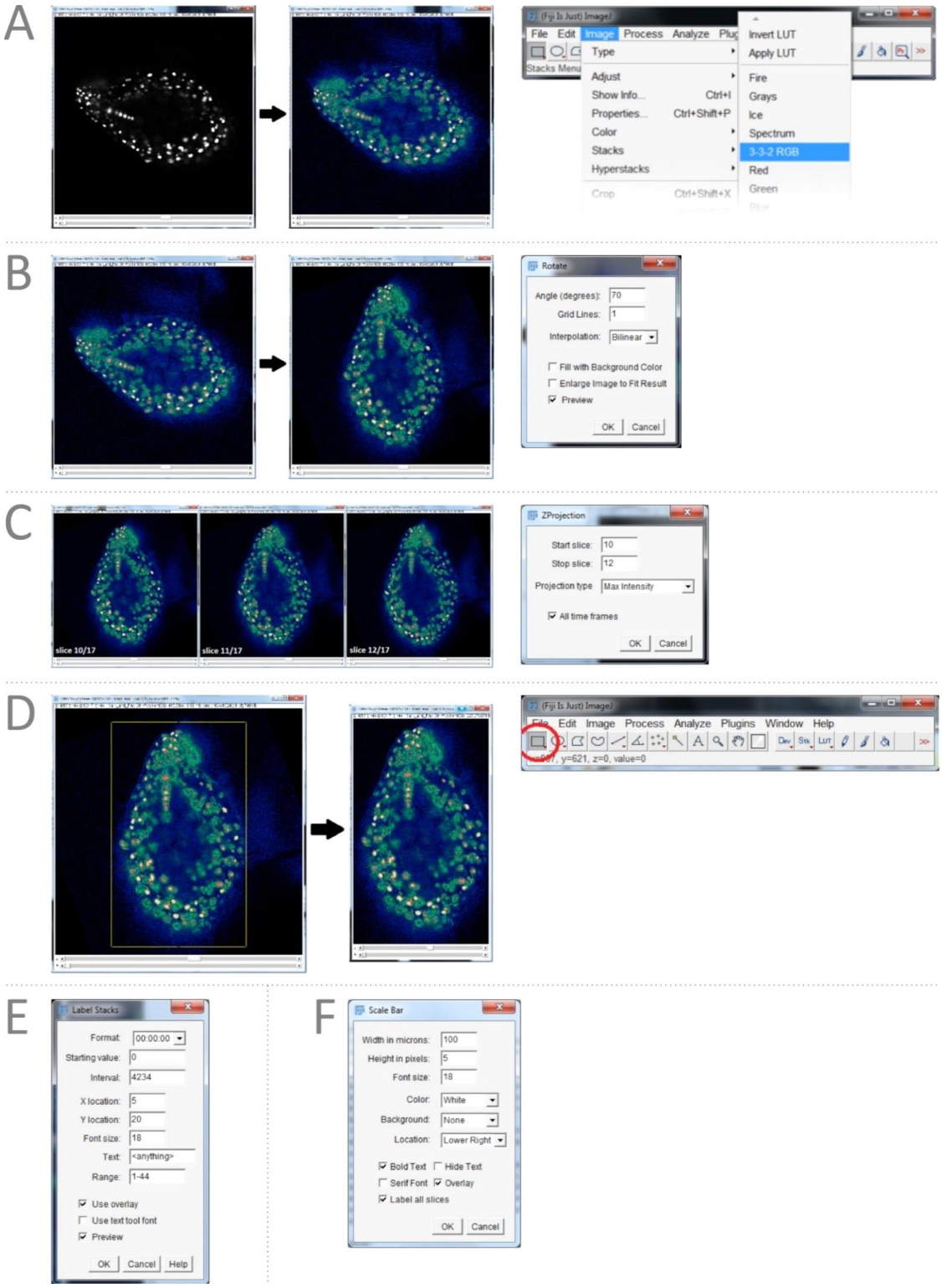

Figuur A8: (A) Applying a LUT-table. (B) Rotating an image. (C) Generating a ZProjection. (D) Cropping an image. (E) Labelling a time-lapse with a time-stamp. (F) Adding a Scale Bar to the image's overlay.

Supplemental tables

Table S1: Ovule growth per ovule position. Data used for **Error! Reference source not found.**. MaAxis and MiAxis change column are colour-oded, low values are red and high values are blue. The difference between MaAxis growth and MiAxis Growth is also colour-coded. Red means that the minor axis grew more in comparison to the major axis, while, conversely, green means that the major axis grew more than the minor axis.

Ovule position number	Length, MaAxis, t=0 (µm)	Length, MiAxis, t=0 (µm)	Length, MaAxis, t=growth time (µm)	Length, MiAxis, t=growth time (µm)	MaAxis change (%)	MiAxis change (%)	Difference, MaAxis Growth-MiAxisGrowth (%)	Growth time (h)	Ecotype
16.3.5	432	268	460	302	6.48%	12.69%	-6.21%	55	Col-0
16.3.6	354	227	365	240	3.11%	5.73%	-2.62%	55	Col-0
16.3.7	349	207	360	220	3.15%	6.28%	-3.13%	55	Col-0
16.3.4	391	234	422	246	7.93%	5.13%	2.80%	55	Col-0
16.3.3	490	331	534	351	8.98%	6.04%	2.94%	55	Col-0
16.3.2	426	254	456	271	7.04%	6.69%	0.35%	55	Col-0
Average	407	254	433	272					
29.3.1	307	173	345	211	12.38%	21.97%	-9.59%	66	Col-0
29.3.3	319	180	363	218	13.79%	21.11%	-7.32%	66	Col-0
29.3.4	244	191	266	237	9.02%	24.08%	-15.07%	66	Col-0
29.3.6	310	196	372	290	20.00%	47.96%	-27.96%	66	Col-0
29.3.7	328	177	417	293	27.13%	65.54%	-38.40%	66	Col-0
29.3.8	344	210	388	233	12.79%	10.95%	1.84%	66	Col-0
29.3.10	320	191	438	280	36.88%	46.60%	-9.72%	66	Col-0
29.3.11	286	185	336	226	17.48%	22.16%	-4.68%	66	Col-0
29.3.12	315	186	375	243	19.05%	30.65%	-11.60%	66	Col-0
29.3.13	288	221	366	242	27.08%	9.50%	17.58%	66	Col-0
29.3.14	418	282	446	294	6.70%	4.26%	2.44%	66	Col-0
29.3.15	477	359	no growth		not included in boxplot, only in averages			66	Col-0
29.3.16	505	354	no growth					66	Col-0
29.3.17	345	201	393	243	13.91%	20.90%	-6.98%	66	Col-0
29.3.18	438	360	501	374	14.38%	3.89%	10.49%	66	Col-0
29.3.19	367	199	410	222	11.72%	11.56%	0.16%	66	Col-0
29.3.20	416	320	475	374	14.18%	16.88%	-2.69%	66	Col-0
29.3.21	307	191	384	323	25.08%	69.11%	-44.03%	66	Col-0
29.3.22	316	173	362	205	14.56%	18.50%	-3.94%	66	Col-0
29.3.23	484	333	529	341	9.30%	2.40%	6.90%	66	Col-0
Average	357	234	398	269					
12.4.2	378	261	432	299	14.29%	14.56%	-0.27%	84	Col-0
12.4.3-1	429	261	464	261	8.16%	0.00%	8.16%	84	Col-0
12.4.3-2	402	263	436	286	8.46%	8.75%	-0.29%	84	Col-0
12.4.4	370	233	425	293	14.86%	25.75%	-10.89%	84	Col-0
12.4.5	419	246	466	272	11.22%	10.57%	0.65%	84	Col-0
12.4.6	358	231	488	354	36.31%	53.25%	-16.93%	84	Col-0
12.4.7	389	324	466	414	19.79%	27.78%	-7.98%	84	Col-0
12.4.8	408	267	478	305	17.16%	14.23%	2.92%	84	Col-0
12.4.10	487	321	572	419	17.45%	30.53%	-13.08%	84	Col-0
12.4.11	413	299	537	388	30.02%	29.77%	0.26%	84	Col-0
12.4.12	482	341	558	327	15.77%	-4.11%	19.87%	84	Col-0
12.4.13	490	376	537	415	9.59%	10.37%	-0.78%	84	Col-0
12.4.14	435	288	493	317	13.33%	10.07%	3.26%	84	Col-0
12.4.17	430	315	474	363	10.23%	15.24%	-5.01%	84	Col-0
12.4.18	477	366	603	398	26.42%	8.74%	17.67%	84	Col-0
12.4.19	455	327	523	351	14.95%	7.34%	7.61%	84	Col-0
12.4.20	474	336	526	393	10.97%	16.96%	-5.99%	84	Col-0
12.4.21	505	348	545	376	7.92%	8.05%	-0.13%	84	Col-0
12.4.22	402	283	542	360	34.83%	27.21%	7.62%	84	Col-0
Average	432	299	503	347					
4.5.1	391	249	425	290	8.70%	16.47%	-7.77%	58	WS
4.5.4	338	195	374	221	10.65%	13.33%	-2.68%	58	WS
4.5.5	334	240	393	270	17.66%	12.50%	5.16%	58	WS
4.5.6	391	257	425	289	8.70%	12.45%	-3.76%	58	WS
4.5.7	359	228	413	251	15.04%	10.09%	4.95%	58	WS
4.5.8	277	169	302	221	9.03%	30.77%	-21.74%	58	WS
4.5.9	403	253	439	275	8.93%	8.70%	0.24%	58	WS
4.5.11	335	234	364	261	8.66%	11.54%	-2.88%	58	WS
4.5.12	313	179	354	235	13.10%	31.28%	-18.19%	58	WS
4.5.13	335	199	386	225	15.22%	13.07%	2.16%	58	WS
4.5.15	420	216	420	195	0.00%	-9.83%	9.83%	58	WS
4.5.17	314	180	369	252	17.52%	40.00%	-22.48%	58	WS
4.5.20	416	222	439	242	5.53%	9.01%	-3.48%	58	WS
4.5.22	310	184	331	194	6.77%	5.43%	1.34%	58	WS
4.5.23	296	229	315	229	6.42%	0.00%	6.42%	58	WS
Average	349	216	383	243					
9.5.5	405	252	430	281	6.17%	11.51%	-5.34%	45	WS
9.5.6	313	222	374	260	19.49%	17.12%	2.37%	45	WS
9.5.7	414	257	440	311	6.28%	21.01%	-14.73%	45	WS
9.5.8	361	270	388	290	7.48%	7.41%	0.07%	45	WS
9.5.10	300	218	365	281	21.67%	28.90%	-7.23%	45	WS
9.5.11	415	252	456	324	9.88%	28.57%	-18.69%	45	WS
Average	**368**	**245**	**409**	**291**					

Table S2: Data per live-imaging experiment. This table continues over this page and the next 3 pages, date imaged is repeated on each page for convenience.

Date plated	Date soiled	Date imaged	Difference, soiled - imaged (days)	Ecotype	Line	Promoter	FP	Line nr.	Plant(s)	Cross	Tier
did not note	5-2-2018	28-2-2018	23	DW	TWIN1	pATPase	Venus	7.3	4	self	3
	5-2-2018	2-3-2018	25	DW	TWIN1	pATPase	Venus	7.3	4	self	3
	5-2-2018	6-3-2018	29	DW	TWIN1	pDRN	Venus	tray678	2	self	3
	5-2-2018	8-3-2018	31	DW	TWIN1	pATPase	Venus	7.3	4	self	3
	5-2-2018	9-3-2018	32	DW	TWIN1	pATPase	Venus	7.3	4	self	3
	5-2-2018	13-3-2018	36	DW	TWIN1	pATPase	Venus	7.3	3, 4	self	3
	1-2-2018	16-3-2018	43	Col-0	M0171	pATPase	Venus	tray677	1, 4	self	2
	1-2-2018	19-3-2018	46	Col-0	M0171	pATPase	Venus	tray677	1, 4	self	2
	17-2-2018	26-3-2018	37	Col-0	M0171	WRKY2	Venus	6,2	3	self	3
	17-2-2018	29-3-2018	40	Col-0	M0171	WRKY2	Venus	6,2	3	UAS-bdl	3
	17-2-2018	29-3-2018	40	Col-0	M0171	WRKY2	Venus	6,2	3 (+3)	self	3
	17-2-2018	12-4-2018	54	Col-0	M0171	WRKY2	Venus	4,3	1	self	3
	5-4-2018	4-5-2018	29	DW	TWIN1	pATPase	Venus	8,4	8, 12, 13	self	2
	5-4-2018	9-5-2018	34	DW	TWIN1	pATPase	Venus	8.4, 6.3	7(6.3); 8, 9, 17(8.4)	self	2
	5-4-2018	11-5-2018	36	DW	TWIN1	pATPase	Venus	8.4, 6.3	7(6.3); 8, 9, 17(8.4)	self	2
31-5-2018	13-6-2018	6-7-2018	23	DW	TWIN1	pATPase	Venus	7,3	6, 14, 15	self	3
15-6-2018	5-7-2018	27-7-2018	22	DW	TWIN1	pATPase	Venus	9,3	7	self	3
5-7-2018	21-8-2018	20-9-2018	30	DW	TWIN1	pATPase	Venus	7,3	**5**	self	3
5-7-2018	21-8-2018	20-9-2018	30	Col-0	M0171	WRKY2	Venus	-	-	UAS-bdl	-
-	-	28-9-2018	-	Col-0	M0171	WRKY2	Venus	-	-	UAS-bdl	-

Date imaged	# ovules screened	# ovules imaged	signal location	# FP signal	%	# suspensor cells @ start	# good or better signal quality (expected)	# good or better signal quality (observed)	# phenotype (expected)	# phenotype (observed)
28-2-2018	11	11	suspensor	3	27%	-	4	0	3	0
2-3-2018	33	23	suspensor	7	21%	-	6	0	3	0
6-3-2018	25	17	proembryo	0	0%	-	0	0	0	0
8-3-2018	14	14	suspensor	5	36%	-	3	3	0	1
9-3-2018	32	14	suspensor	11	34%	-	6	6	4	0
13-3-2018	33	7	suspensor	4	12%	-	0	0	0	0
16-3-2018	26	8	micropillar endosperm	8	31%	-	0	0	wt	wt
19-3-2018	40	8	suspensor	0	0%	-	0	0	wt	wt
26-3-2018	36	26	suspensor	20	56%	-	13	13	wt	wt
29-3-2018	21	10	suspensor	11	52%	7	5	5	GAL4 silenced	GAL4 silenced
29-3-2018	29	13	suspensor	8	28%	4	5	5	wt	wt
12-4-2018	29	19	suspensor	0	0%	-	0	0	wt	wt
4-5-2018	66	28	suspensor	20	30%	5	18	18	13	6
9-5-2018	78	15	suspensor	14	18%	5	8	8	9	8
11-5-2018	15	6	suspensor	6	40%	8	6	6	6	6
6-7-2018	85	18	suspensor	17	20%	4	14	14	12	6
27-7-2018	47	30	suspensor	19	40%	5	13	13	6	1
20-9-2018	38	1	suspensor	1	3%	-	-	-	-	0
20-9-2018	40	0	suspensor	0	0%	-	-	-	-	-
28-9-2018	78	24	suspensor	12	15%	-	-	5	-	2

Date imaged	# aborted ovules	%	t, screen(h)	t, measurement(h)	τ, max(h)	τ, avg(h)	avg. Length major axis, t=0 (µm)	avg. Length minor axis, t=0 (µm)	avg. Length major axis, t=end (µm)	avg. Length minor axis, t=end (µm)	Plate contam.	Medium contam.
28-2-2018	didn't check			12	3	3	no growth				-	☒
2-3-2018	didn't check			24	24	19	no growth				☒	☒
6-3-2018	5	20%	15	12	no signal		no growth				-	☒
8-3-2018	7	50%	14	11	11	11	no growth				☒	☒
9-3-2018	6	19%	62	28	28	27	no growth				☒	☒
13-3-2018	12	36%	15	12	13	4	no growth				-	☒
16-3-2018	23	88%	60	55	55	49	407	254	433	272	-	☒
19-3-2018	13	33%	14	12	no signal		no growth				-	☒
26-3-2018	6	17%	22	11	41	35	no growth				-	☒
29-3-2018	5	24%	87	66	110	106	357	234	398	269	-	☒
29-3-2018	13	45%	87	66	110	76					-	☒
12-4-2018	13	45%	86	84	no signal		426	299	503	347	-	☒
4-5-2018	8	12%	62	58	58	44	349	216	383	243	-	☒
9-5-2018	14	18%	110	45	45	34	368	245	409	291	-	☒
11-5-2018	same as (9-5-18)			60	60	45	zoom too large				-	☒
6-7-2018	24	28%	68	54	59	33	zoom too large				-	☒
27-7-2018	20	43%	62	60	60	38	zoom too large				-	☒
20-9-2018	-	-	-	21	21	21	zoom too large				-	☒
20-9-2018	-	-	-	-	-	-	zoom too large				-	☒
28-9-2018	-	-	-	62	62	-	zoom too large				-	☒

Date imaged	objective	immersion	WLL Power (%)	scan speed (Hz)	Scan direction X	pinhole size (µm)	HyD (nr.)	resolution	Zoom (x)	laser power (%)	gain (%)	λ, excitation (nm)	λ, emission. Range (nm)	z-stack step size (µm)	line average	frame average	Bright R (on/off)	Filesize (GB)	t, interval (min)	devices used (amount * nr)
28-2-2018	20x	20% glycerol	50	400	Unidirectional	60,7	3	512x512	0,75	21	100	514	520-601	9.52-16.67	1	1	☒	0,5	30	1x300
2-3-2018	20x	20% glycerol	50	400	Unidirectional	38,0	3	512x512	0,99	17	100	514	520-601	6.03-13.11	1	1	☒	1,2	60	2x300
6-3-2018	20x	20% glycerol	50	400	Unidirectional	60,7	2	1024x1024	0,8	21	100	514	517-580	10	8	1	☒	2,3	64	2x300
8-3-2018	20x	20% glycerol	50	400	Unidirectional	60,7	2	1024x1024	1,25	45	100	514	551-611	10	1	1	☒	1,6	60	1x300
9-3-2018	20x	20% glycerol	50	400	Unidirectional	60,7	2	1024x1024	1,15	43	100	514	551-601	10	1	1	☒	5,4	70	2x300
13-3-2018	20x	20% glycerol	50	400	Unidirectional	60,7	2	1024x1024	1,25	21	100	514	550-600	10	1	1	☒	1,4	60	2x300
16-3-2018	20x	20% glycerol	50	400	Unidirectional	60,7	2	1024x1024	1,11	26	100	514	560-602	10	8	1	☒	1,1	408	1x300
19-3-2018	20x	20% glycerol	50	400	Unidirectional	60,7	2	1024x1024	1	32	100	514	549-603	10	8	1	☒	1,5	60	1z300
26-3-2018	20x	20% glycerol	50	400	Unidirectional	60,7	2	1024x1024	1	60	100	514	549-603	10	8	1	☒	2,6	76	3x300
29-3-2018	20x	20% glycerol	50	400	Unidirectional	60,7	2	1024x1024	1	60	100	514	549-603	10	8	1	☒	12,3	83	1x300
29-3-2018	20x	20% glycerol	50	400	Unidirectional	60,7	2	1024x1024	1	60	100	514	549-603	10	8	1	☒	12,3	83	1x300
12-4-2018	20x	20% glycerol	50	400	Unidirectional	60,7	2	1024x1024	1	49	100	514	520-601	10	8	1	☒	15,6	77	1x350; 1x300
4-5-2018	20x	20% glycerol	50	400	Unidirectional	60,7	3	1024x1024	1,4	61	100	514	545-610	10	1	1	☒	10,7	84	1x350; 2x300
9-5-2018	20x	20% glycerol	50	400	Unidirectional	60,7	3	1024x1024	1,4	35	100	514	534-584	10	1	1	☑	8,6	70	1x350; 3x300
11-5-2018	20x	20% glycerol	50	400	Unidirectional	60,7	3	1024x1024	2,8	35	100	514	534-584	5	1	1	☑	8,9	30	1x350; 3x300
6-7-2018	20x	20% glycerol	50	400	Unidirectional	60,7	2	2048x2048	2,75	25	150	514	535-570	10	1	4	☑	42,4	64	2x350; 2x300
27-7-2018	20x	20% glycerol	50	400	Bidirectional X, Phase: 32.13	60,7	2	1024x1024	3	35	100	514	535-560	5 or 10	8	0	☒	15,4	60	4x300
20-9-2018	20x	20% glycerol	50	200	Bidirectional X, Phase: 32.14	60,7	2	1024x1024	2.25	35	100	514	535-560	5	1	8	☒	1,9	15,8	1x350
20-9-2018	20x	20% glycerol	50	-	-	60,7	2	-	-	-	-	-	-	-	-	-	☒	-	-	-
28-9-2018	20x	20% glycerol	50	400 to 200	Bidirectional X, Phase: 32.16	60,7	2	1024x1024	1,65 to 2,4	35	100	514	535-560	5 or 10	8	1	☒	21,1	45 to 30	3x350, 1x300

Table S3: Number of suspensor cells with fluorescent signal per position. Position numbers are the same in corresponding .lit files. The number of suspensor cells could be off because sometimes not all cells have a fluorescent signal or not all cells are visible. Why this is useful? Maybe for estimating embryo stage or estimating at what number of suspensor cells wrong divisions occur most of and from there determine whether wrong divisions could have occurred in the first place during live-imaging of the respective ovule. The latter could be included in estimating twin phenotype penetrance.

Position/Date	29-3-2018	29-3-2018	12-4-2018	4-5-2018	9-5-2018	11-5-2018	6-7-2018	27-7-2018
1		4		5			5	
2				4	5	10	2	6
3		5		5	4		4	
4				5	6		2	5
5				5	3		5	
6		7		8	6	6	5	3
7		6		8	8	10		
8		7			9		6	6
9		6		6	5		2	2
10		6		3	4	5	2	
11		5		6			2	5
12		6		3			6	4
13		6			4	7	3	7
14	4			7	5		2	7
15	4			6	5		6	6
16	4			4			2	
17				6			5	5
18	4			4			4	
19				4				5
20	3			5				
21	6			4				6
22	5							4
23	4			7				
24								6
25				4				
26								
27								5
28								5
29								6
30								9

Table S4: Fluorescent signal quality as observed per ovule position. Quality numbering range from 0-4. 0 being the worst, 4 being optimal.

Position/Date	28-2-2018	2-3-2018	6-3-2018	8-3-2018	9-3-2018	13-3-2018	16-3-2018	19-3-2018	26-3-2018	29-3-2018	29-3-2018	12-4-2018	4-5-2018	9-5-2018	11-5-2018	6-7-2018	27-7-2018
1					3	1	no suspensor signal → micropillar endosperm lifetime measured, quality of micropillar signal is equal in every ovule	no suspensor signal	2		2	no signal observed	4	0		2	
2	2			3					1				3	4	4	3	3
3											2		4	2		1	
4			1						4		1		4	4	2	4	3
5	2				1				4				4	3		4	
6	1	0			1	1			3		3		4	4	4	4	2
7	2		1		3				2		1		4	4	4	0	
8	1	1	1		4	1					4			2		4	4
9		0			3	1					4		4	2		4	2
10			1	1	4						2			4	4	2	2
11				0	0				1		2		3	0		3	
12		1			2				3		4		4	0		4	1
13		2		4	0				2		4			4	3	3	3
14				4	3					3			4	3		3	3
15			1		2				1	4			4	2		3	4
16									2	3			3			3	
17		1							3				4			4	3
18		1							3	1			4			3	
19													1				3
20									2	1			4				
21									3	4			1				3
22									3	3							3
23									4	2			4				
24									3								3
25									3				3				
26		-							3								
27																	4
28																	2
29																	4
30																	2

Table S5: Fluorescent signal lifetime per ovule position. Dates with an * were checked for a signal post-live-imaging; that is why signal lifetimes are up to 110 hours.

Position /Date	28-2-2018	2-3-2018	6-3-2018	8-3-2018	9-3-2018	13-3-2018	16-3-2018	19-3-2018	26-3-2018 *	29-3-2018 *	29-3-2018 *	12-4-2018	4-5-2018	9-5-2018	11-5-2018	6-7-2018	27-7-2018
1	glycerol evaporation				28		51	no signal	12		110	no signal	58			13	
2				11			48		41		110		58	45	49	10	28
3							48				110		57	19		4	
4			12				48		41		66.3		10	35	15	59	60
5							55		41				52	34		59	
6		24				4	48		41		110		40	18	60	34	8
7					28		48		12				55	45	60	0	
8					28	4					110			15		59	60
9					28						110		58	45		59	48
10				11	28						110			45	42		
11									41		110		50				17
12		20			20				12		110		58				17
13				11					41		110			45	42		31
14				11	27					110			46	42			37
15			12		28				41	28			17	18			38
16									41	47			32				
17		24							41				58				48
18		18							41	110			58				
19																	31
20									41	31			40				
21									12	110							54
22									12	110							53
23									41	66			44				
24									41								44
25									41				6				
26		11							41								
27																	41
28																	42
29																	29

Table S6: phenotype per ovule position. 0 is no phenotype, 1 is phenotype.

Position/Date	28-2-2018	2-3-2018	6-3-2018	8-3-2018	9-3-2018	13-3-2018	16-3-2018	19-3-2018	26-3-2018	29-3-2018	29-3-2018	12-4-2018	4-5-2018	9-5-2018	11-5-2018	6-7-2018	27-7-2018
1	0	0	0	0	0								0			0	0
2	0	0	0	0	0								0	1	1	0	0
3	0	0	0	0	0								1	0		0	0
4	0	0	0	0									1	1	1	0	0
5	0	0	0	0	0								0	0		1	0
6	0	0	0	0	0								0	1	1	0	0
7	0	0	0	0	0								0	1	1		0
8	0	0	0	0	0								0	1		1	0
9		0	0	0	1								0	0		0	0
10		0	0	0	0								0	1	1	0	0
11		0	0	0	0								0	0		1	0
12		0	0	0	0								0	0		1	0
13		0	0	0	0								0	1	1	0	0
14		-	0	0	0								1	1		1	0
15		0	0		0				**WT plants**				1	0		0	0
16		0	0										0			0	0
17		0	0										0			1	0
18		0											0			0	0
19		0											0				0
20		0											1				0
21		0											0				0
22		0											0				1
23		0											1				0
24		0											0				1
25													1				0
26													0				0
27													0				0
28													0				0
29																	1
30																	0

References

Berleth, T., & Chatfield, S. (2002). Embryogenesis: pattern formation from a single cell. *The Arabidopsis Book*, 1–22. https://doi.org/10.1199/tab.0051

Dharmasiri, N., Dharmasiri, S., Weijers, D., Lechner, E., Yamada, M., Hobbie, L., … Estelle, M. (2005). Plant development is regulated by a family of auxin receptor F box proteins. *Developmental Cell*, *9*(1), 109–119. https://doi.org/10.1016/j.devcel.2005.05.014

Friml, J., Benková, E., Blilou, I., Wisniewska, J., Hamann, T., Ljung, K., … Sandberg, G. (2002). AtPIN4 Mediates Sink-Driven Auxin Gradients and Root Patterning in Arabidopsis suggest the involvement of the phytohormone auxin in this process. Here, we characterize a novel member of the PIN family of putative auxin efflux carriers, Arabi. *Cell*, *108*, 661–673.

Gooh, K., Ueda, M., Aruga, K., Park, J., Arata, H., Higashiyama, T., & Kurihara, D. (2015). Live-Cell Imaging and Optical Manipulation of Arabidopsis Early Embryogenesis. *Developmental Cell*, *34*(2), 242–251. https://doi.org/10.1016/j.devcel.2015.06.008

Park, J., Kurihara, D., Higashiyama, T., & Arata, H. (2014). Fabrication of microcage arrays to fix plant ovules for long-term live imaging and observation. *Sensors and Actuators, B: Chemical*, *191*, 178–185. https://doi.org/10.1016/j.snb.2013.09.060

Rademacher, E. H., Lokerse, A. S., Schlereth, A., Llavata-Peris, C. I., Bayer, M., Kientz, M., … Weijers, D. (2012). Different Auxin Response Machineries Control Distinct Cell Fates in the Early Plant Embryo. *Developmental Cell*, *22*(1), 211–222. https://doi.org/10.1016/j.devcel.2011.10.026

Radoeva, T. (2016). *Mechanistic dissection of plant embryo initiation*.

Smyth, D. R. (1990). Early Flower Development in Arabidopsis. *The Plant Cell Online*, *2*(8), 755–767. https://doi.org/10.1105/tpc.2.8.755

Srivastava, D., & DeWitt, N. (2016). In Vivo Cellular Reprogramming: The Next Generation. *Cell*, *166*(6), 1386–1396. https://doi.org/10.1016/j.cell.2016.08.055

Ueda, M., Zhang, Z., & Laux, T. (2011a). Transcriptional Activation of Arabidopsis Axis Patterning Genes WOX8/9 Links Zygote Polarity to Embryo Development. *Developmental Cell*, *20*(2), 264–270. https://doi.org/10.1016/j.devcel.2011.01.009

Ueda, M., Zhang, Z., & Laux, T. (2011b). Transcriptional Activation of Arabidopsis Axis Patterning Genes WOX8/9 Links Zygote Polarity to Embryo Development. *Developmental Cell*, *20*(2), 264–270. https://doi.org/10.1016/j.devcel.2011.01.009

Vernon & Meinke, D. M. & D. W. (1994). Embryogenic Tranformation of the Suspensor in twin, a Polyembryonic Mutant of Arabidopsis. Oklahoma: Developmental Biology.

Waldchen, S., Lehmann, J., Klein, T., Van De Linde, S., & Sauer, M. (2015). Light-induced cell damage in live-cell super-resolution microscopy. *Scientific Reports*, *5*, 1–12. https://doi.org/10.1038/srep15348

Yeung, E. C. (1993). Embryogenesis in Angiosperms: Development of the Suspensor. *The Plant Cell Online*, *5*(10), 1371–1381. https://doi.org/10.1105/tpc.5.10.1371